

IN CONCLUSION,
AAAAAAA!!!



THE BEST THESIS DEFENSE IS A GOOD THESIS OFFENSE.

Applications of Computation in Acoustics: Ultrasound Bioeffects & Underwater Transmission Loss Uncertainty

A *dissertation defense* by:
Brandon Patterson

Scientific Computing and Flow Physics Lab
University of Michigan, Ann Arbor
Department of Mechanical Engineering

October 31, 2017



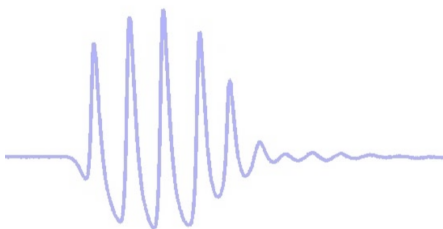
My dissertation: Computational techniques and modeling to solve modern problems in acoustics

Two somewhat different areas of acoustics

Acoustic uncertainty in the ocean



Ultrasound bioeffects



My dissertation: Computational techniques and modeling to solve modern problems in acoustics

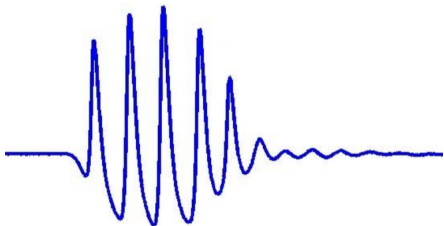
Two somewhat different areas of acoustics

Acoustic uncertainty in the ocean



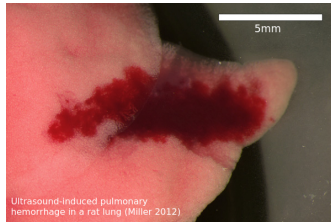
static.pexels.com

Ultrasound bioeffects

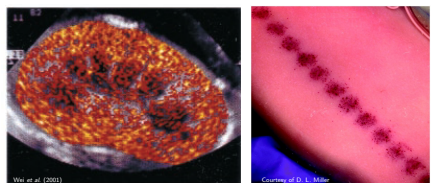


Part I: Diagnostic ultrasound bioeffects

Ultrasound-induced
lung hemorrhage

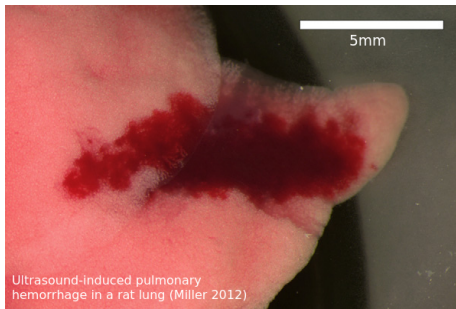


Contrast-enhanced ultrasound:
Cavitation bioeffects



Diagnostic ultrasound can trigger lung hemorrhage in mammals

- Diagnostic lung ultrasound is increasingly common in critical care scenarios (Lichtenstein, 2009)
- Lung hemorrhage, the only known bioeffect of non-contrast DUS, has been observed in mice, rats, pigs, rabbits, monkeys (Child *et al.*, 1990; O'Brien & Zachary, 1997; Tarantal & Canfield, 1994).
- The underlying physical damage mechanism is poorly understood.



We aim to study the physics underlying ultrasound-alveolar interactions

- 1.) Develop a physics based model of ultrasound-alveolar interactions

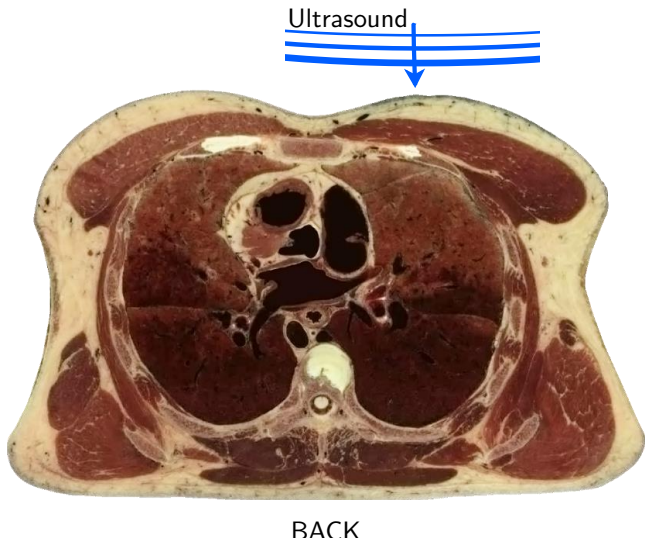
We aim to study the physics underlying ultrasound-alveolar interactions

- 1.) Develop a physics based model of ultrasound-alveolar interactions
- 2.) Describe the dynamics in terms of the driving physical mechanisms

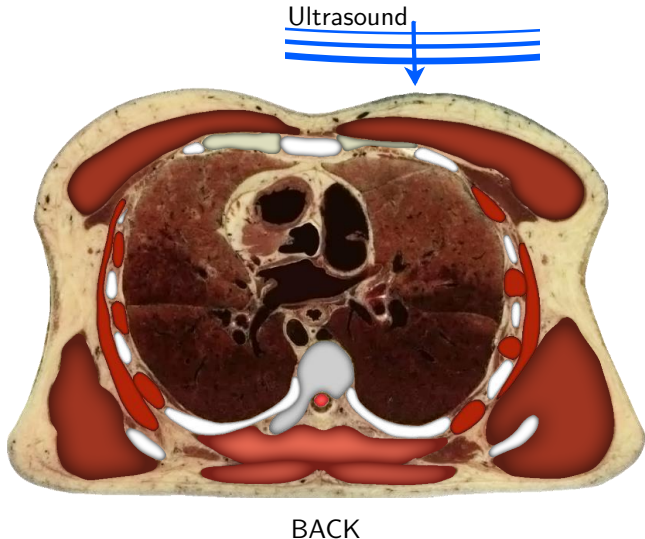
We aim to study the physics underlying ultrasound-alveolar interactions

- 1.) Develop a physics based model of ultrasound-alveolar interactions
- 2.) Describe the dynamics in terms of the driving physical mechanisms
- 3.) Use the model to determine possible hemorrhage mechanisms.
 - Estimate alveolar stresses and strains relevant to diagnostic US
 - Compare results with possible damage thresholds

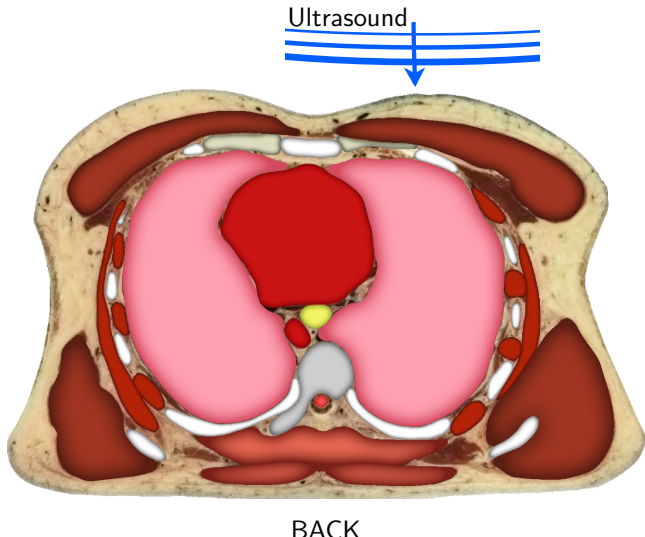
Lets consider the physical problem



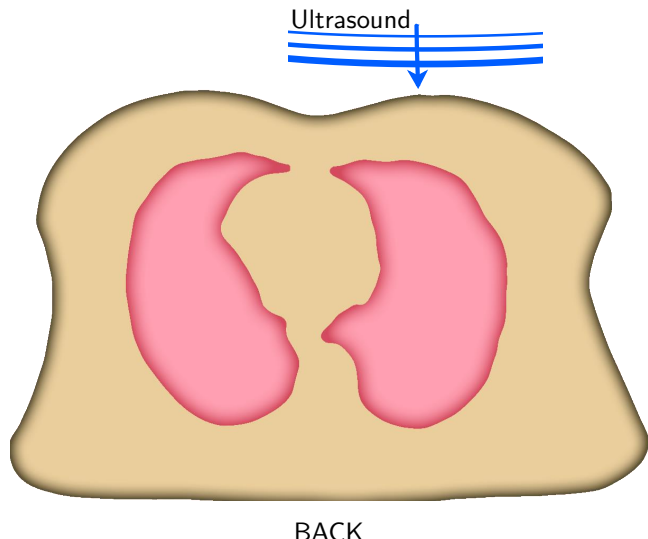
Lets consider the physical problem



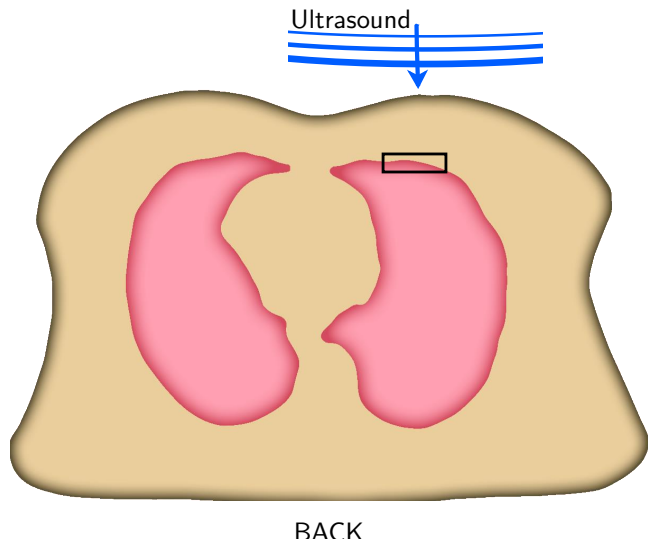
Lets consider the physical problem



Lets consider the physical problem

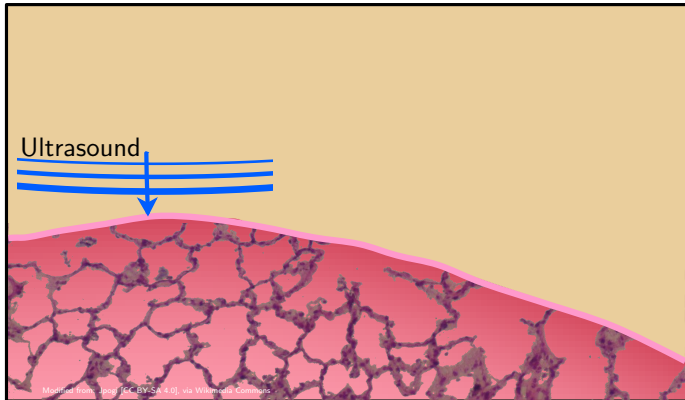


Lets consider the physical problem

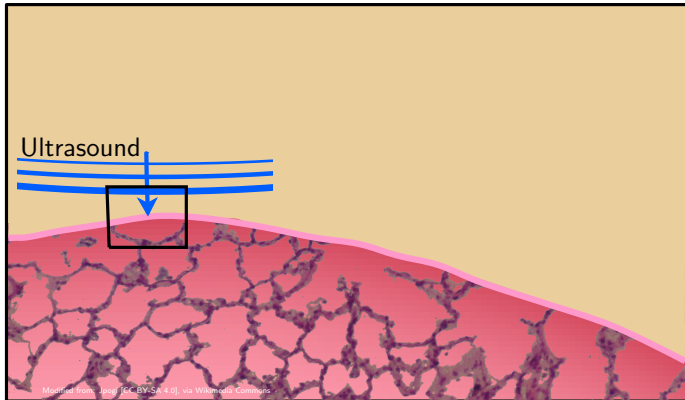


BACK

Lets consider the physical problem



Lets consider the physical problem



Developing and justifying the model problem

Soft tissue: ρ, μ, E

Ultrasound: p_a, f

Tissue-air
interface

Alveolus (air)



ℓ

Developing and justifying the model problem

Soft tissue: ρ, μ, E

Ultrasound: p_a, f

Tissue-air
interface

Alveolus (air)

ℓ

Length scales

Physical	Length	Length (ℓ)
Alveolar diameter, ℓ	200 μm	1ℓ
Thoracic wall	$\sim 4 \text{ cm}$	200ℓ
Alveolar wall	$\lesssim 1 \mu\text{m}$	$\ll 1\ell$
US wavelength, λ	$\sim 1 \text{ mm}$	5ℓ
US pulse length	9 mm	45ℓ

Developing and justifying the model problem

Soft tissue: ρ, μ, E

Ultrasound: p_a, f

Tissue-air
interface

Alveolus (air)

ℓ

Length scales

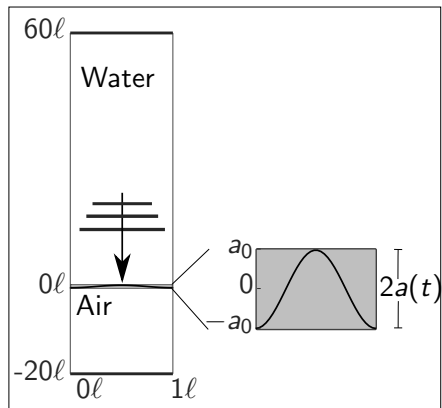
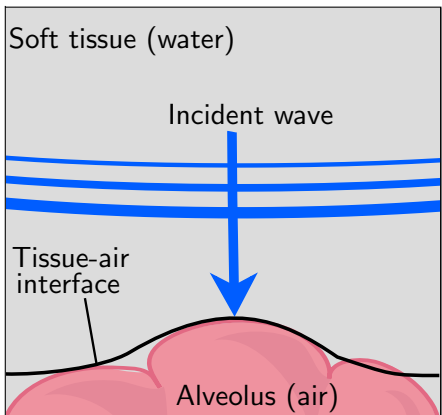
Physical	Length	Length (ℓ)
Alveolar diameter, ℓ	200 μm	1ℓ
Thoracic wall	$\sim 4 \text{ cm}$	200ℓ
Alveolar wall	$\lesssim 1 \mu\text{m}$	$\ll 1\ell$
US wavelength, λ	$\sim 1 \text{ mm}$	5ℓ
US pulse length	9 mm	45ℓ

Dimensional analysis

Physical property	Dimensionless scale
$\text{Re} = \rho u \ell / \mu$	$= \mathcal{O}(10^4)$
$\text{Ca} = \mu u^2 / E$	$= \mathcal{O}(10^2)$
$\text{We} = \rho u^2 \ell / S$	$= \mathcal{O}(10^4)$
$\text{Fr} = u / \sqrt{g \ell}$	$= \mathcal{O}(10^2)$

$$\rho = 1000 \frac{\text{m}}{\text{s}}, E = 5 \text{kPa}, S = 9 \frac{\text{mN}}{\text{m}}, u = 31.6 \frac{\text{m}}{\text{s}}$$

Problem setup: We model the ultrasound-alveolar interaction as a 2D, compressible, inviscid fluid system.



Governing Equations

Euler equations of fluid motion

$$\frac{\partial \rho}{\partial t} + \frac{\partial (\rho u)}{\partial x} + \frac{\partial (\rho v)}{\partial y} = 0, \quad \text{Continuity}$$

$$\frac{\partial \rho u}{\partial t} + \frac{\partial}{\partial x} \left(\rho u^2 + p \right) + \frac{\partial}{\partial y} (\rho u v) = 0, \quad x\text{-momentum}$$

$$\frac{\partial \rho v}{\partial t} + \frac{\partial}{\partial x} (\rho u v) + \frac{\partial}{\partial y} \left(\rho v^2 + p \right) = 0, \quad y\text{-momentum}$$

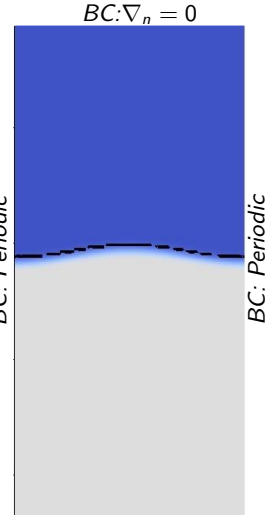
$$\frac{\partial E}{\partial t} + \frac{\partial}{\partial x} [u(E + p)] + \frac{\partial}{\partial y} [v(E + p)] = 0, \quad \text{Energy}$$

Stiffened equation of state

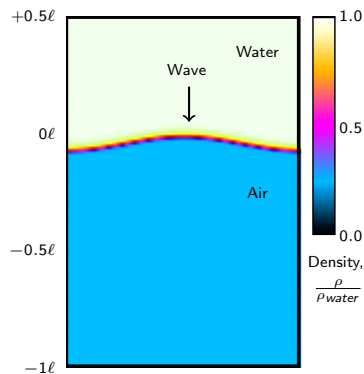
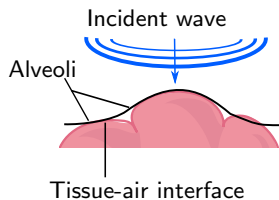
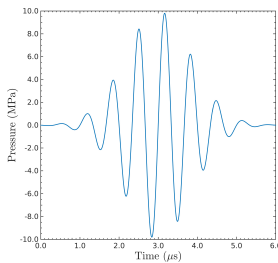
$$E = \frac{\rho(u^2 + v^2)}{2} + \frac{p + \gamma B}{\gamma - 1}.$$

A high-order accurate computational solution strategy is invoked

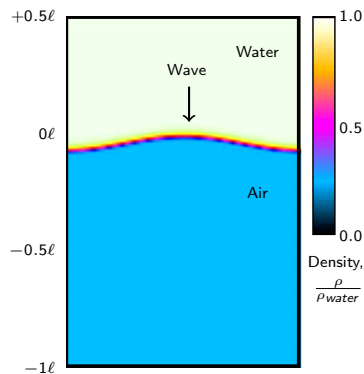
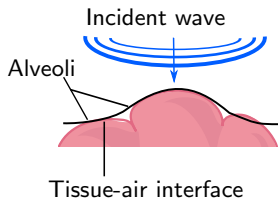
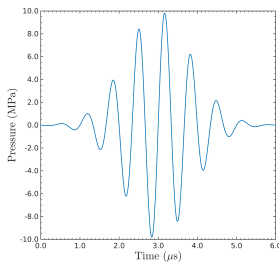
- An in-house developed code is used to solve the Euler equations.
- Numerical methods (Henry de Franan *et al.*, 2015)
 - 3rd order Discontinuous Galerkin method used in space
 - 4th order Runge-Kutta time marching
 - Roe Solver used for fluxes
- Acoustic waves prescribed in the domain.
- Grid stretching reduces reflections.
- Grid size: $\ell \times 80\ell$ ($L_x \times L_y$)



We simulated and US-pulse impinging on a water-air interface



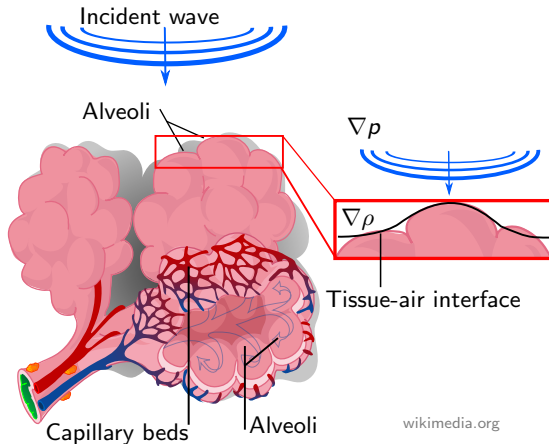
We simulated and US-pulse impinging on a water-air interface



- Linear acoustics doesn't explain the interface deformation

$$\left(\frac{a_0}{u_{\text{wave}}} = 0.01a_0 = \mathcal{O}(10^{-7}) \text{ m} \right).$$

We hypothesize that US waves generate baroclinic vorticity at gas-liquid interfaces, driving deformation.

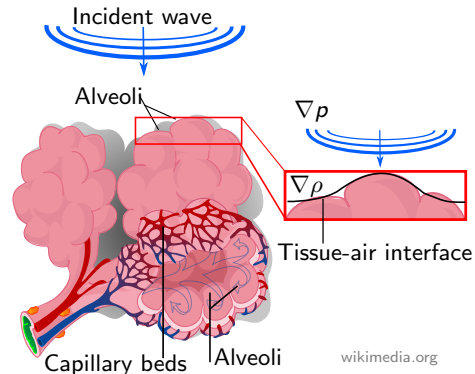


We hypothesize that US waves generate baroclinic vorticity at gas-liquid interfaces, driving deformation.

The vorticity generation equation

$$\frac{D\omega}{Dt} = (\boldsymbol{\omega} \cdot \nabla) \mathbf{u} - \boldsymbol{\omega} (\nabla \cdot \mathbf{u}) + \frac{\nabla p \times \nabla p}{\rho^2} - \nabla \times \left(\frac{\nabla \cdot \boldsymbol{\tau}}{\rho} \right) + \nabla \times \mathbf{B}$$

material derivative stretching compressibility baroclinic viscous body forces

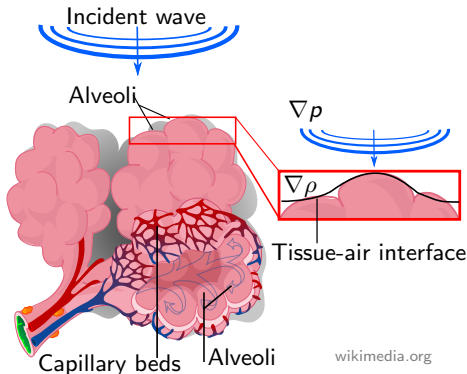


We hypothesize that US waves generate baroclinic vorticity at gas-liquid interfaces, driving deformation.

The vorticity generation equation

$$\frac{D\omega}{Dt} = \cancel{(\omega \cdot \nabla) u}^{\sim 0} - \cancel{\omega (\nabla \cdot u)}^{\sim 0} + \frac{\nabla p \times \nabla p}{\rho^2} - \nabla \times \left(\frac{\nabla \cdot r}{\rho} \right)^{\sim 0} + \nabla \times \mathbf{B}^{\sim 0}$$

material derivative stretching compressibility baroclinic viscous body forces



wikimedia.org

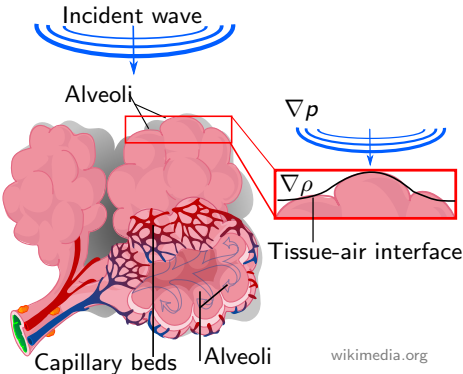
We hypothesize that US waves generate baroclinic vorticity at gas-liquid interfaces, driving deformation.

The vorticity generation equation

$$\frac{D\omega}{Dt} = (\omega \cdot \nabla) \mathbf{u}^{\sim 0} - \omega (\nabla \cdot \mathbf{u})^{\sim 0} + \frac{\nabla p \times \nabla p}{\rho^2} - \nabla \times \left(\frac{\nabla \tau}{\rho} \right)^{\sim 0} + \nabla \times \mathbf{B}^{\sim 0}$$

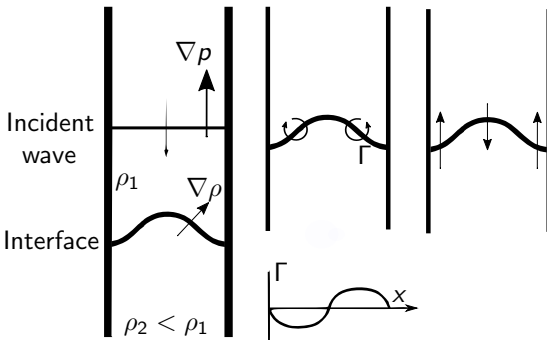
material derivative stretching compressibility baroclinic viscous body forces

- Air-tissue interfaces have sharp density gradients
- US has strong pressure gradients
- US-induced baroclinic vorticity may strain interface, *similar to shock-driven interfaces*
- Linear acoustics does not capture this.

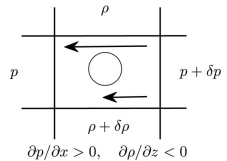


wikimedia.org

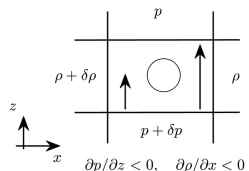
Shock-driven fluid-fluid interfaces have been studied extensively



Adapted from Brouillette (2002)



$$\frac{\partial p}{\partial x} > 0, \quad \frac{\partial \rho}{\partial z} < 0$$

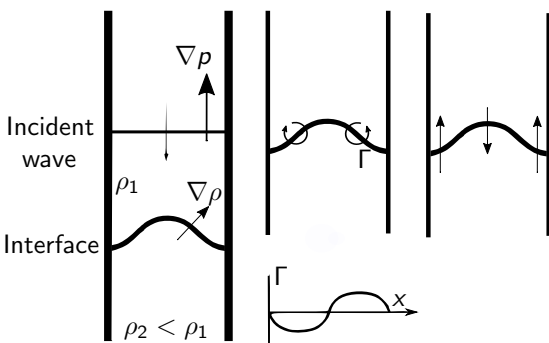


$$\frac{\partial p}{\partial z} < 0, \quad \frac{\partial \rho}{\partial x} < 0$$

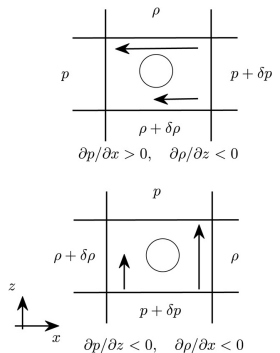
Adapted from Heifetz & Mak (2015)

- Shocks deposit baroclinic vorticity at perturbed fluid interfaces (Drake, 2006).

Shock-driven fluid-fluid interfaces have been studied extensively



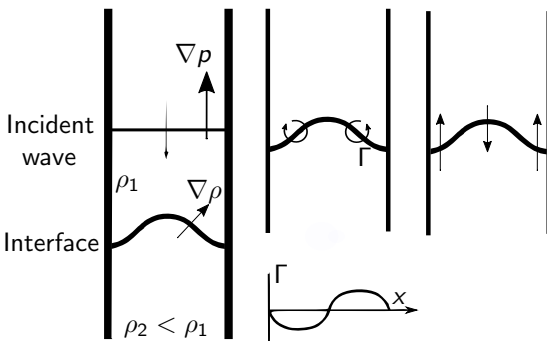
Adapted from Brouillette (2002)



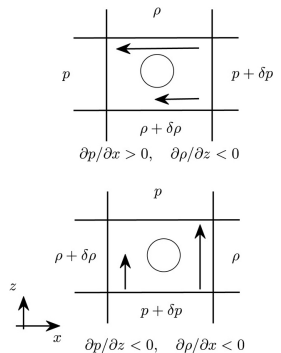
Adapted from Heifetz & Mak (2015)

- Shocks deposit baroclinic vorticity at perturbed fluid interfaces (Drake, 2006).
- This vorticity drives the interface perturbation to grow.

Shock-driven fluid-fluid interfaces have been studied extensively



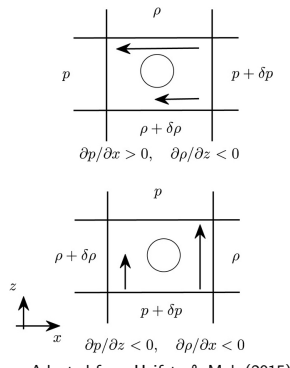
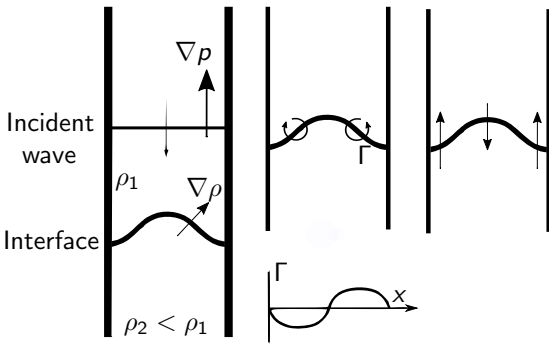
Adapted from Brouillette (2002)



Adapted from Heifetz & Mak (2015)

- Shocks deposit baroclinic vorticity at perturbed fluid interfaces (Drake, 2006).
- This vorticity drives the interface perturbation to grow.
- This is the Richtmyer-Meshkov “instability”.

Shock-driven fluid-fluid interfaces have been studied extensively



- Shocks deposit baroclinic vorticity at perturbed fluid interfaces (Drake, 2006).
- This vorticity drives the interface perturbation to grow.
- This is the Richtmyer-Meshkov “instability”.
- Acoustic waves are different. They interact over a finite time-scale.

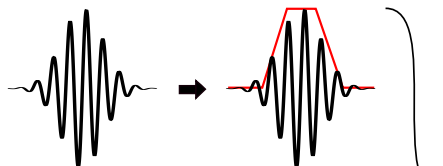
Revised research plan

First: Develop a simplified problem to study the fluid mechanics

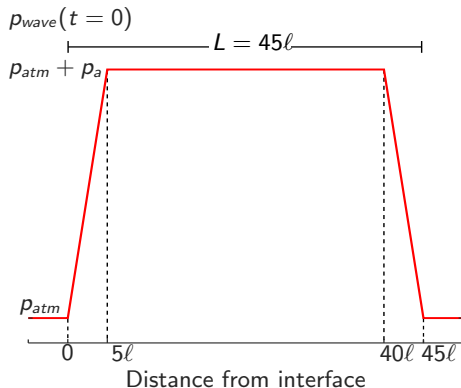
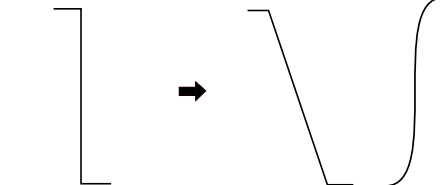
Second: Return to the diagnostic ultrasound pulse to study possible relevance to ultrasound-induced lung hemorrhage.

A trapezoidal acoustic wave is used to study the physics

Ultrasound Pulse

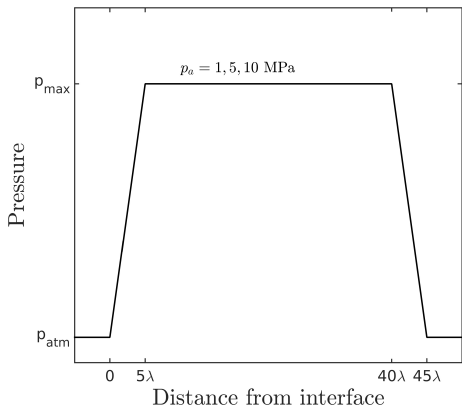
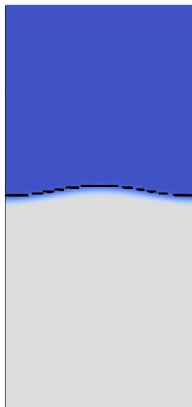


Shock wave



- Symmetric in time
- Returns to ambient pressure
- Well-prescribed pressure gradients

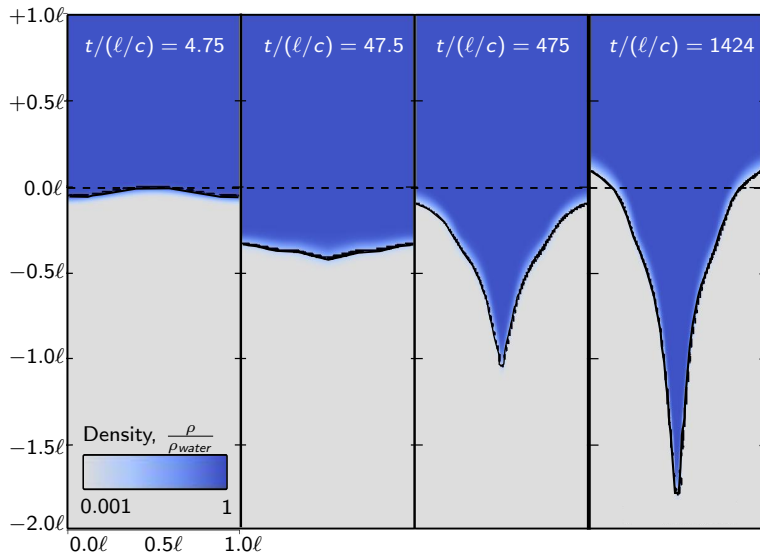
The baseline case: a 10 MPa trapezoidal wave hits a nearly-flat sinusoidal interface



$$a_0 = 0.03\ell$$

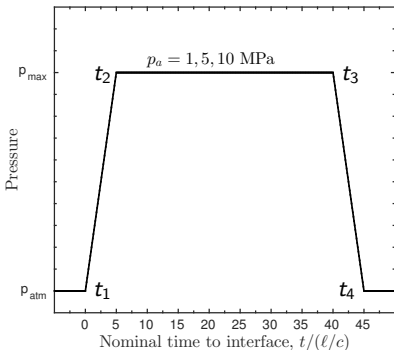
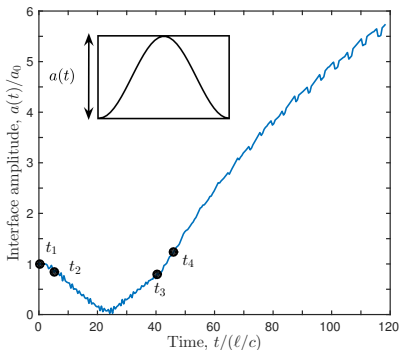
$$p_a = 10 \text{ MPa}, L = 45\ell$$

Results: Evolution of the interface for the 10 MPa trapezoidal wave



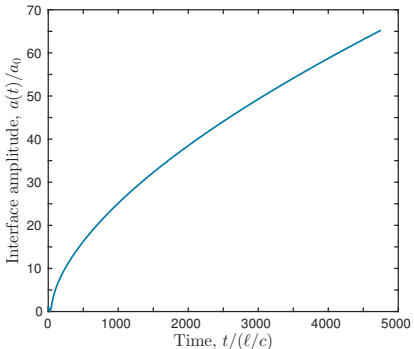
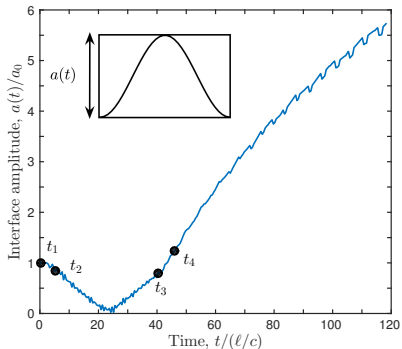
The interface perturbation evolves from a smooth sinusoid into a sharp point.

Results: Growth of the interface perturbation



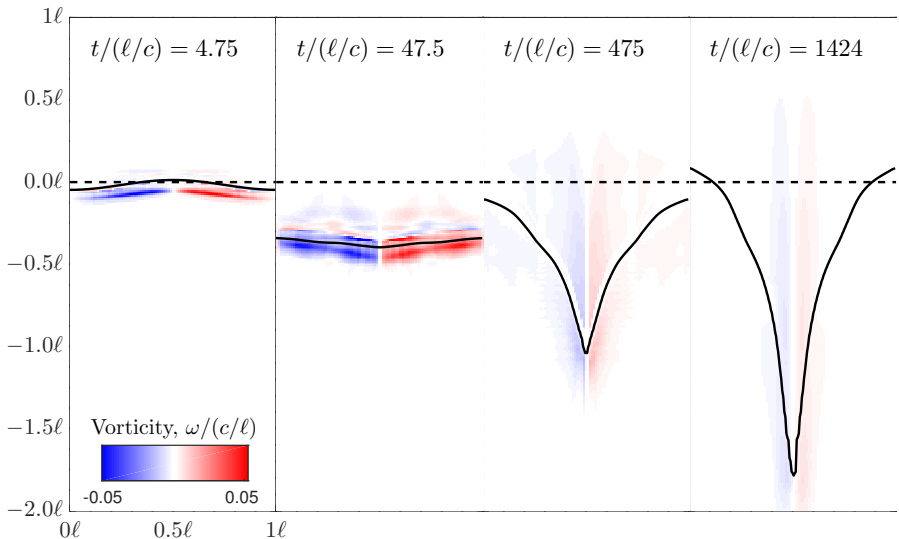
The interface perturbation is initially compressed: $0^+ \leq t/(\ell/c) \leq 24$; experiences a phase change at $t/(\ell/c) \approx 24$, then grows: $t/(\ell/c) > 24$.

Results: Growth of the interface perturbation



The interface perturbation continues to grow at late times, long after the wave has passed. Eventually, the growth appears asymptotic.

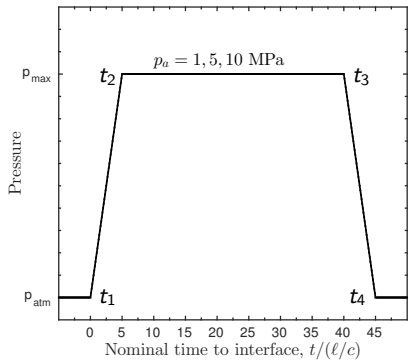
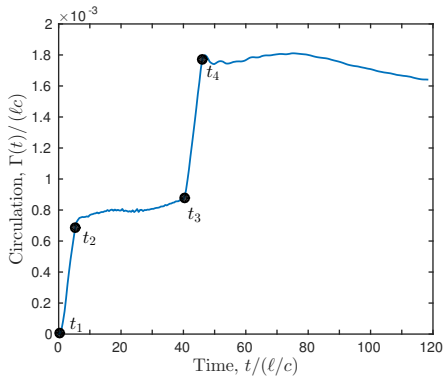
Results: Evolution of the vorticity for the 10 MPa trapezoidal wave



Vorticity ($\omega = \nabla \times \mathbf{u}$) is deposited by the wave and remains after the wave passes.

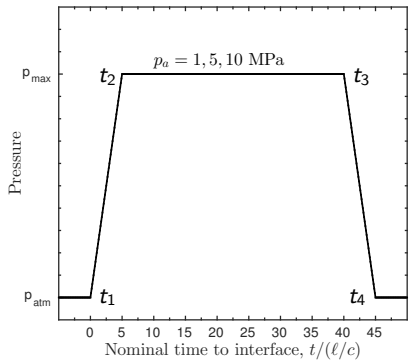
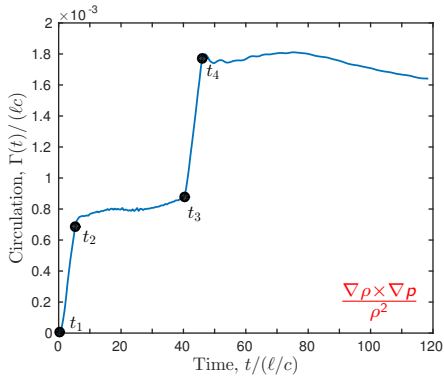
Results: Circulation deposited by the 10 MPa trapezoidal wave

$$\Gamma(t) = \int_{A_R} \omega_z(\mathbf{x}, t) dA_R$$



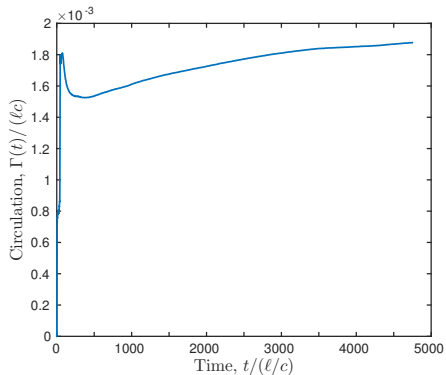
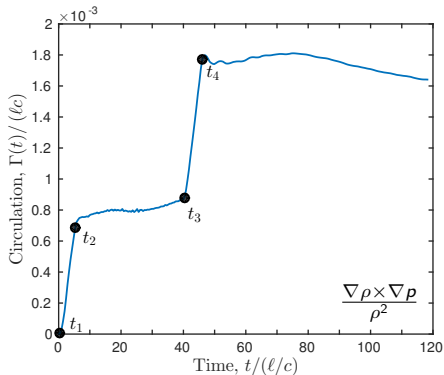
Results: Circulation deposited by the 10 MPa trapezoidal wave

$$\Gamma(t) = \int_{A_R} \omega_z(\mathbf{x}, t) dA_R$$



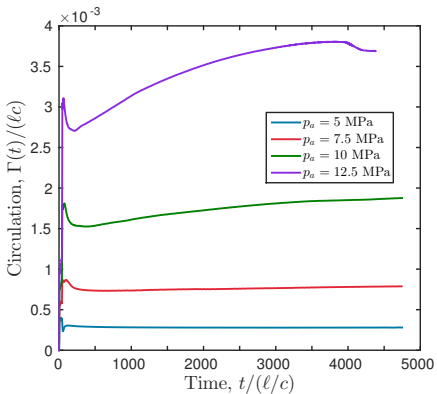
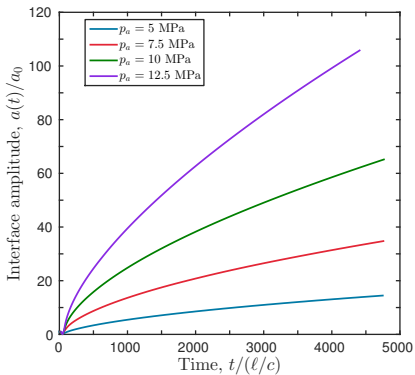
Results: Circulation deposited by the 10 MPa trapezoidal wave

$$\Gamma(t) = \int_{A_R} \omega_z(\mathbf{x}, t) dA_R$$



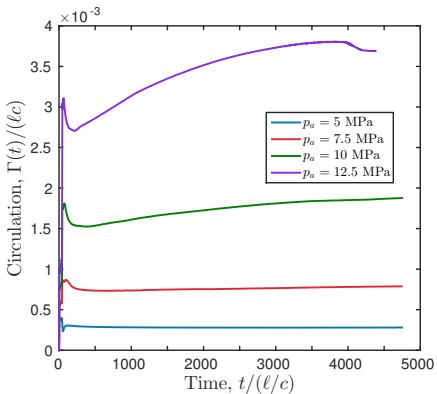
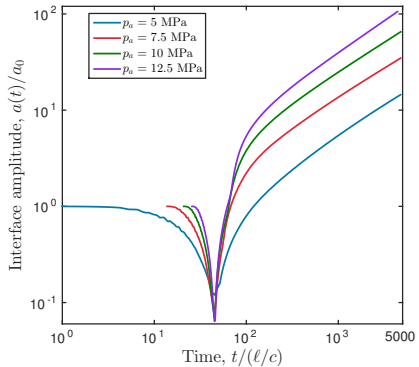
Acoustically-generated circulation remains after the passage of the wave.

Results: dependence of perturbation growth $a(t)$, circulation $\Gamma(t)$ on wave amplitude $p_a = 5$ to 12.5 MPa



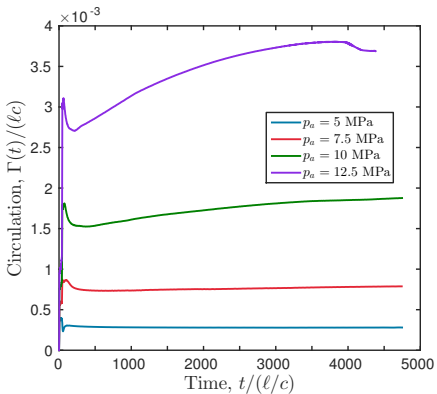
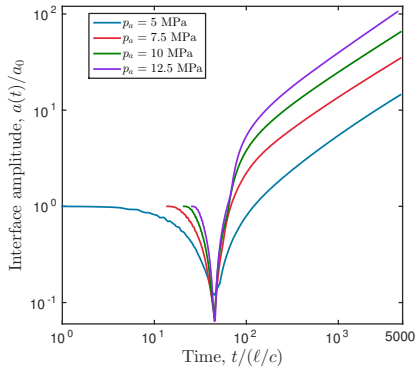
- Asymptotic late-time growth observed for all wave amplitudes
- Lasting circulation deposited for all wave amplitudes

Results: dependence of perturbation growth $a(t)$, circulation $\Gamma(t)$ on wave amplitude $p_a = 5$ to 12.5 MPa



- Asymptotic late-time growth observed for all wave amplitudes
- Lasting circulation deposited for all wave amplitudes

Results: dependence of perturbation growth $a(t)$, circulation $\Gamma(t)$ on wave amplitude $p_a = 5$ to 12.5 MPa

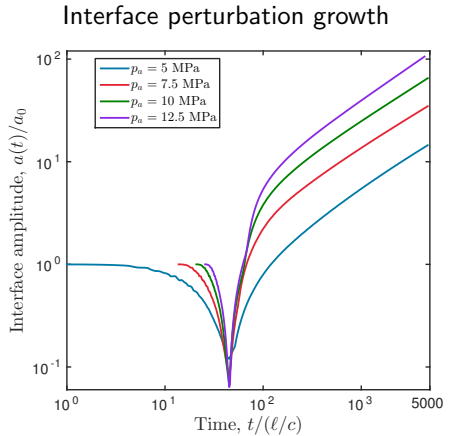


- Asymptotic late-time growth observed for all wave amplitudes
- Lasting circulation deposited for all wave amplitudes
- I aim to explain this growth

Dimensional analysis and explanation of the perturbation growth

Perturbation amplitude dependencies:

$$a(t) = f(\Gamma, s, \ell, c; t)$$



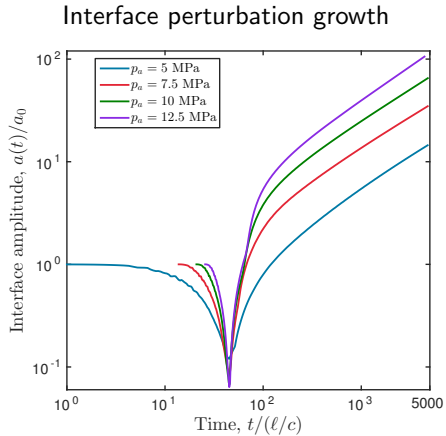
Dimensional analysis and explanation of the perturbation growth

Perturbation amplitude dependencies:

$$a(t) = f(\Gamma, s, \ell, c; t)$$

Non-dimensionalize:

$$\frac{a(t)}{\ell} = G \left(\frac{\Gamma}{\ell c}, \frac{s}{\ell}; \frac{t}{\ell/c} \right)$$



Dimensional analysis and explanation of the perturbation growth

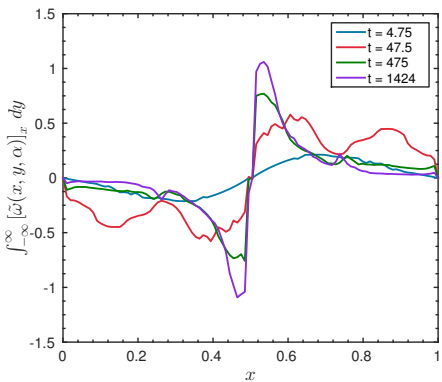
Perturbation amplitude dependencies:

$$a(t) = f(\Gamma, s, \ell, c; t)$$

Non-dimensionalize:

$$\frac{a(t)}{\ell} = G \left(\frac{\Gamma}{\ell c}, \frac{s}{\ell}; \frac{t}{\ell/c} \right)$$

Vorticity redistributes itself



Suggests Γ/s is important

Dimensional analysis and explanation of the perturbation growth

Perturbation amplitude dependencies:

$$a(t) = f(\Gamma, s, \ell, c; t)$$

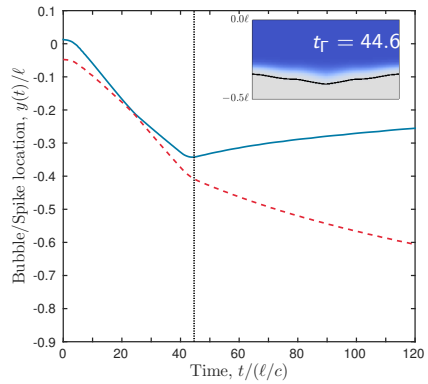
Non-dimensionalize:

$$\frac{a(t)}{\ell} = G \left(\frac{\Gamma}{\ell c}, \frac{s}{\ell}; \frac{t}{\ell/c} \right)$$

Scale by physically meaningful terms:

$$\frac{a(t)}{\ell} = \frac{\Gamma_0}{s_0 c} \mathcal{F} \left(\frac{tc}{\ell} \right).$$

Bubble reverses against the wave



$$\left. \frac{\Gamma}{s} \right|_{t_\Gamma=44.6} = \frac{\Gamma_0}{s_0}$$

Dimensional analysis and explanation of the perturbation growth

Perturbation amplitude dependencies:

$$a(t) = f(\Gamma, s, \ell, c; t)$$

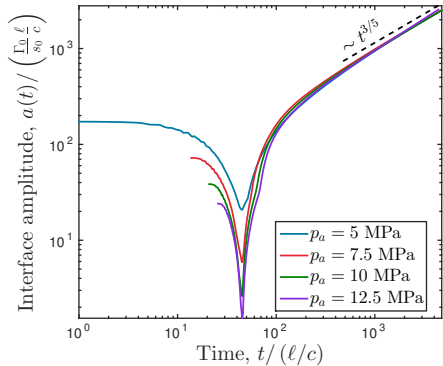
Non-dimensionalize:

$$\frac{a(t)}{\ell} = G \left(\frac{\Gamma}{\ell c}, \frac{s}{\ell}; \frac{t}{\ell/c} \right)$$

Scale by physically meaningful terms:

$$\frac{a(t)}{\ell} = \frac{\Gamma_0}{s_0 c} \mathcal{F} \left(\frac{tc}{\ell} \right).$$

The scaled curves collapse



$$a(t) \sim t^{3/5}$$

Dimensional analysis and explanation of the perturbation growth

Perturbation amplitude dependencies:

$$a(t) = f(\Gamma, s, \ell, c; t)$$

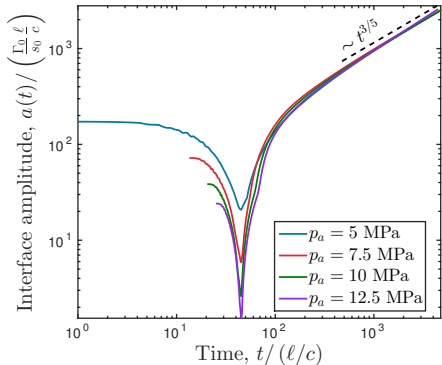
Non-dimensionalize:

$$\frac{a(t)}{\ell} = G \left(\frac{\Gamma}{\ell c}, \frac{s}{\ell}; \frac{t}{\ell/c} \right)$$

Scale by physically meaningful terms:

$$\frac{a(t)}{\ell} = \frac{\Gamma_0}{s_0 c} \mathcal{F} \left(\frac{tc}{\ell} \right).$$

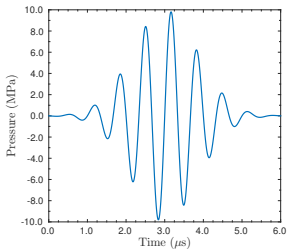
The scaled curves collapse



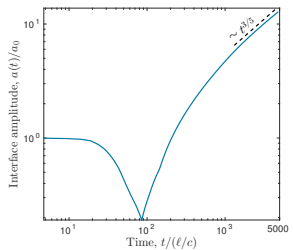
$$a(t) \sim t^{3/5}$$

The interface perturbation growth scales with circulation density, and is therefore vorticity driven.

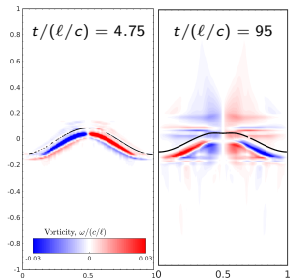
We see similar growth from the US wave



Ultrasound pulse



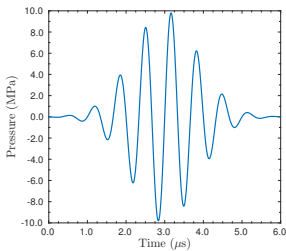
Interface growth $a(t)/a_0$



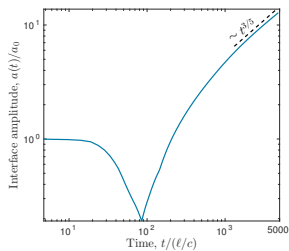
Vorticity

$p_a = 10$ MPa ultrasound pulse results in similar interface growth and vorticity to the trapezoidal wave.

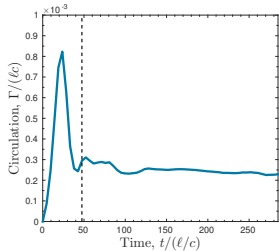
We see similar growth from the US wave



Ultrasound pulse



Interface growth $a(t)/a_0$

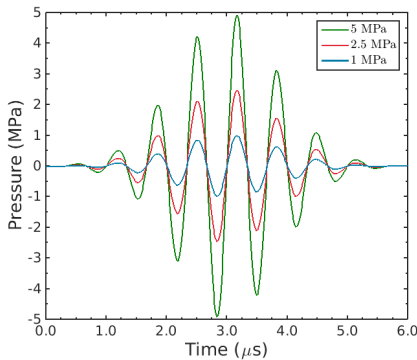


Circulation, $\Gamma/(\ell c)$

$p_a = 10$ MPa ultrasound pulse results in similar interface growth and vorticity to the trapezoidal wave.

Now let's consider the more clinically relevant cases

Wave and interface perturbation amplitudes are varied.

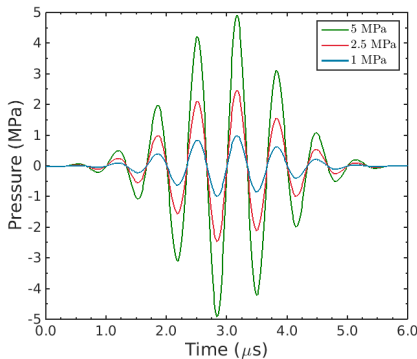


Ultrasound Pulses

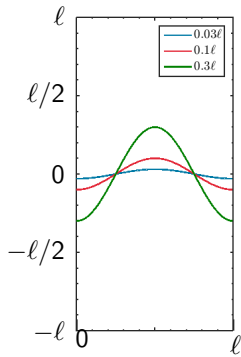
- Assume typical alveolar diameter $\ell = 200\mu\text{m}$ (Ochs *et al.*, 2004)
- Pulse amplitudes, $p_a = 1, 2.5, 5 \text{ MPa}$; frequency, $f = 1.5 \text{ MHz}$

Now let's consider the more clinically relevant cases

Wave and interface perturbation amplitudes are varied.



Ultrasound Pulses



Interface initial conditions

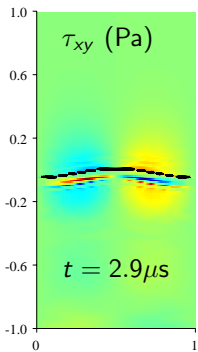
- Assume typical alveolar diameter $\ell = 200\mu\text{m}$ (Ochs *et al.*, 2004)
- Pulse amplitudes, $p_a = 1, 2.5, 5 \text{ MPa}$; frequency, $f = 1.5 \text{ MHz}$

The inferred viscous stress is calculated

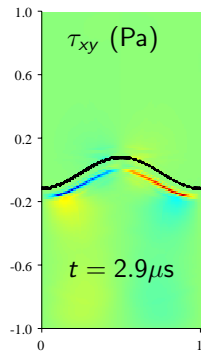
$$\tilde{\mu} = \alpha \mu_{water} + (1 - \alpha) \mu_{air}, \quad \tau_{xy}(x, y, t) = \tilde{\mu} \left(\frac{\partial u}{\partial y} + \frac{\partial v}{\partial x} \right), \quad p_a = 5 \text{ MPa}$$

The inferred viscous stress is calculated

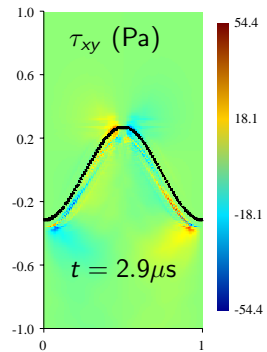
$$\tilde{\mu} = \alpha \mu_{water} + (1 - \alpha) \mu_{air}, \quad \tau_{xy}(x, y, t) = \tilde{\mu} \left(\frac{\partial u}{\partial y} + \frac{\partial v}{\partial x} \right), \quad p_a = 5 \text{ MPa}$$



$$a_0 = 0.03\ell$$



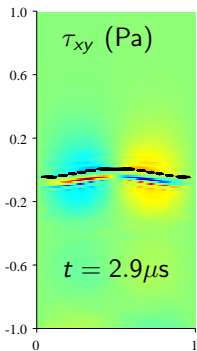
$$a_0 = 0.1\ell$$



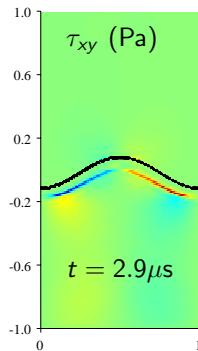
$$a_0 = 0.3\ell$$

The inferred viscous stress is calculated

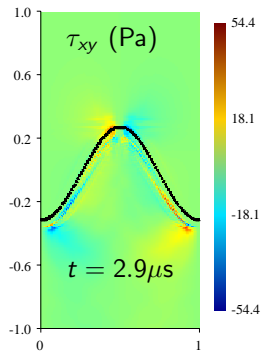
$$\tilde{\mu} = \alpha \mu_{water} + (1 - \alpha) \mu_{air}, \quad \tau_{xy}(x, y, t) = \tilde{\mu} \left(\frac{\partial u}{\partial y} + \frac{\partial v}{\partial x} \right), \quad p_a = 5 \text{ MPa}$$



$$a_0 = 0.03\ell$$



$$a_0 = 0.1\ell$$



$$a_0 = 0.3\ell$$

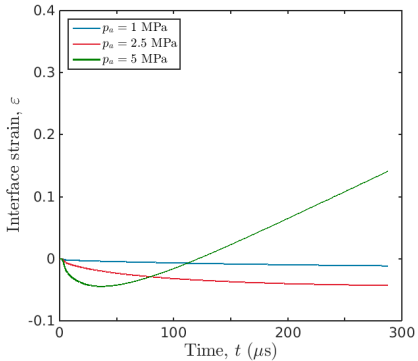
- Viscous shear stresses are concentrated at the interface
- The maximum shear stress, occurs with the peak negative pressure

The interface strain is calculated

$$\varepsilon(t) = \frac{s(t) - s_0}{s_0}, \quad s = \text{arclength of interface}$$

The interface strain is calculated

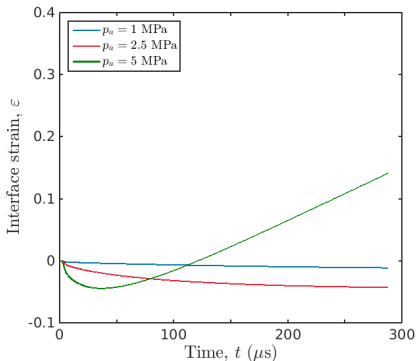
$$\varepsilon(t) = \frac{s(t) - s_0}{s_0}, \quad s = \text{arclength of interface}$$



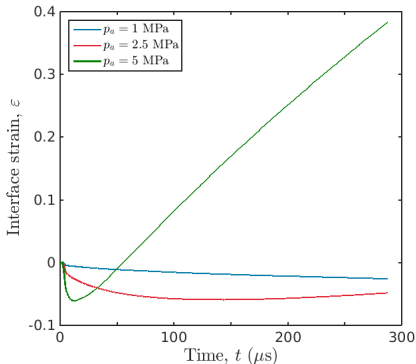
$$a_0 = 0.1\ell$$

The interface strain is calculated

$$\varepsilon(t) = \frac{s(t) - s_0}{s_0}, \quad s = \text{arclength of interface}$$



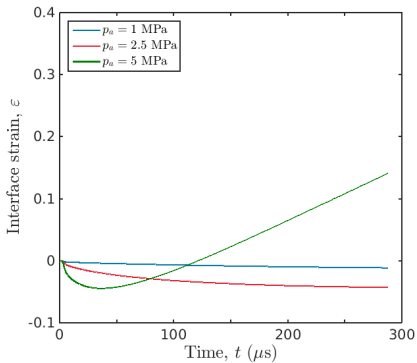
$$a_0 = 0.1\ell$$



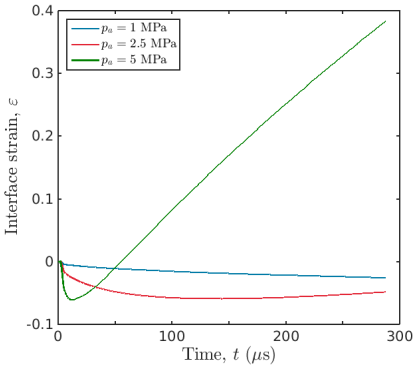
$$a_0 = 0.3\ell$$

The interface strain is calculated

$$\varepsilon(t) = \frac{s(t) - s_0}{s_0}, \quad s = \text{arclength of interface}$$



$$a_0 = 0.1\ell$$



$$a_0 = 0.3\ell$$

- Strain increases with increasing p_a and a_0
- Strains up to 38% observed ($a_0 = 0.3\ell$; $p_a = 5 \text{ MPa}$) at $t \approx 300\mu\text{s}$.
- \approx alveolar strain failure criterion, $\varepsilon = ?$.

Discussion and limitations of these results

- Late-time behavior may not be captured by this model because elasticity, viscosity, surface tension and failure are likely to play a greater role.
- Actual diagnostic ultrasound relies on multiple pulses and the vorticity driving the interface strain has the potential to accumulate from pulse to pulse ($\ell^2/v_{air} \sim \mathcal{O}(ms)$).

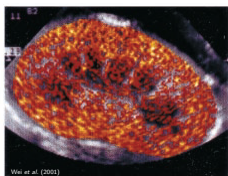
Conclusions about acoustically-driven liquid-gas interfaces and ultrasound-induced lung hemorrhage

- 1.) Acoustic waves may generate sufficient baroclinic vorticity at gas-liquid interfaces to drive perturbation growth.
- 2.) This perturbation growth exhibits power-law behavior in time.
- 3.) Diagnostic ultrasound pulses may drive significant strains at alveolar interfaces through cumulative vorticity deposition, possibly causing hemorrhage.
- 4.) Viscous shear stress due to ultrasound is likely too small to cause alveolar hemorrhage.

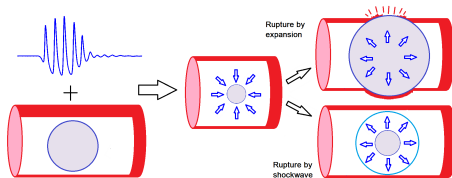
Part I, Problem 2

Contrast-enhanced ultrasound (CEUS) bioeffects

Background on contrast-enhanced ultrasound bioeffects



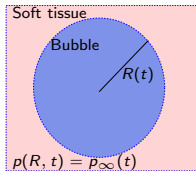
Wei et al. (2001)



- Contrast-Ehanced Ultrasound (CEUS) provides high contrast diagnostic medical imaging in areas without high contrast (e.g., blood).
- CEUS uses echogenic microbubbles for contrast, and can lead to hemorrhage and cell death.
- Though cavitation of the microbubbles appears to be the cause, the exact mechanisms and thresholds are not well understood.

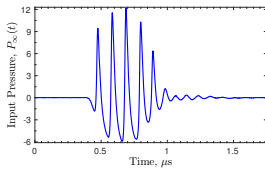
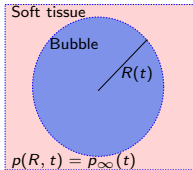
The goal was to study the relationship between theoretical microbubble dynamics and experimental bioeffects thresholds

We model spherical bubble dynamics in compressible, viscoelastic soft tissue, driven by experimentally-measured US waves with known bioeffects thresholds (Miller,2008;Patterson,2012)



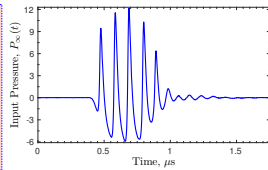
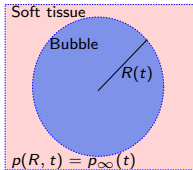
The goal was to study the relationship between theoretical microbubble dynamics and experimental bioeffects thresholds

We model spherical bubble dynamics in compressible, viscoelastic soft tissue, driven by experimentally-measured US waves with known bioeffects thresholds (Miller,2008;Patterson,2012)



The goal was to study the relationship between theoretical microbubble dynamics and experimental bioeffects thresholds

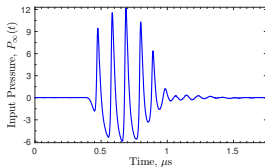
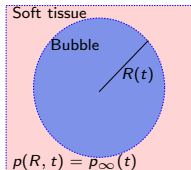
We model spherical bubble dynamics in compressible, viscoelastic soft tissue, driven by experimentally-measured US waves with known bioeffects thresholds (Miller,2008;Patterson,2012)



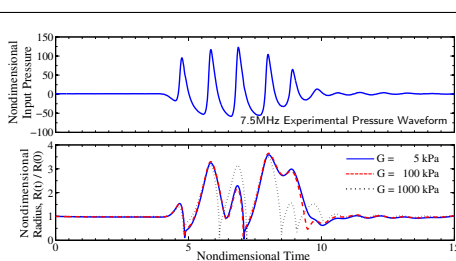
$$\begin{aligned} \left(1 - \frac{\dot{R}}{C}\right) R \ddot{R} + \frac{3}{2} \left(1 - \frac{\dot{R}}{3C}\right) \dot{R}^2 &= \\ \left(1 + \frac{\dot{R}}{C}\right) \left[p_B - 1 - p_\infty - \frac{R}{C} \frac{dp_\infty}{dt} \right] + \frac{R}{C} \dot{p}_B, \\ p_B &= \left(1 + \frac{2}{We}\right) \frac{1}{R^{3\gamma}} - \frac{2}{WeR} + \tau_R, \end{aligned}$$

The goal was to study the relationship between theoretical microbubble dynamics and experimental bioeffects thresholds

We model spherical bubble dynamics in compressible, viscoelastic soft tissue, driven by experimentally-measured US waves with known bioeffects thresholds (Miller, 2008; Patterson, 2012)

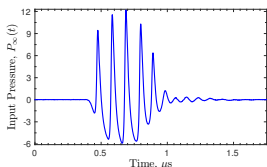
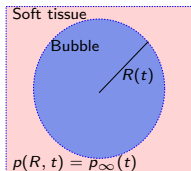


$$\left(1 - \frac{\dot{R}}{C}\right) R \ddot{R} + \frac{3}{2} \left(1 - \frac{\dot{R}}{3C}\right) \dot{R}^2 = \\ \left(1 + \frac{\dot{R}}{C}\right) [p_B - 1 - p_\infty - \frac{R}{C} \frac{dp_\infty}{dt}] + \frac{R}{C} \dot{p}_B,$$
$$p_B = \left(1 + \frac{2}{We}\right) \frac{1}{R^{3\gamma}} - \frac{2}{WeR} + \tau_R,$$

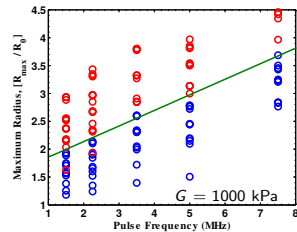
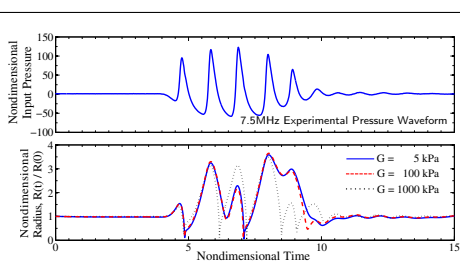


The goal was to study the relationship between theoretical microbubble dynamics and experimental bioeffects thresholds

We model spherical bubble dynamics in compressible, viscoelastic soft tissue, driven by experimentally-measured US waves with known bioeffects thresholds (Miller, 2008; Patterson, 2012)

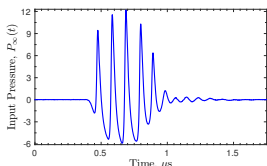
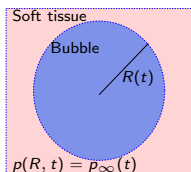


$$\left(1 - \frac{\dot{R}}{C}\right) R \ddot{R} + \frac{3}{2} \left(1 - \frac{\dot{R}}{3C}\right) \dot{R}^2 = \\ \left(1 + \frac{\dot{R}}{C}\right) [p_B - 1 - p_\infty - \frac{R}{C} \frac{dp_\infty}{dt}] + \frac{R}{C} \dot{p}_B,$$
$$p_B = \left(1 + \frac{2}{We}\right) \frac{1}{R^{3\gamma}} - \frac{2}{WeR} + \tau_R,$$

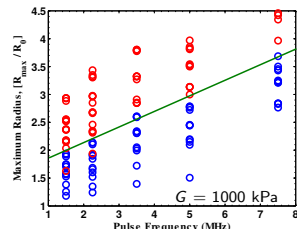
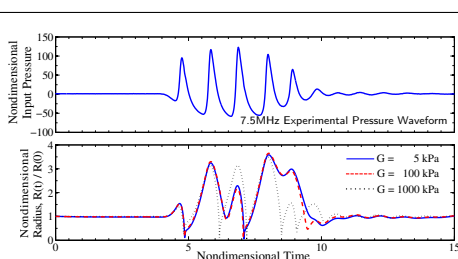


The goal was to study the relationship between theoretical microbubble dynamics and experimental bioeffects thresholds

We model spherical bubble dynamics in compressible, viscoelastic soft tissue, driven by experimentally-measured US waves with known bioeffects thresholds (Miller, 2008; Patterson, 2012)



$$\left(1 - \frac{\dot{R}}{C}\right) R \ddot{R} + \frac{3}{2} \left(1 - \frac{\dot{R}}{3C}\right) \dot{R}^2 = \\ \left(1 + \frac{\dot{R}}{C}\right) \left[p_B - 1 - p_\infty - \frac{R}{C} \frac{dp_\infty}{dt} \right] + \frac{R}{C} \dot{p}_B, \\ p_B = \left(1 + \frac{2}{We}\right) \frac{1}{R^{3\gamma}} - \frac{2}{WeR} + \tau_R,$$



Calculated cavitation metrics (e.g., R_{\max}/R_0) clearly separate cases for which experimental bioeffects thresholds were / were not observed.

Part II:

Underwater acoustic transmission loss uncertainty

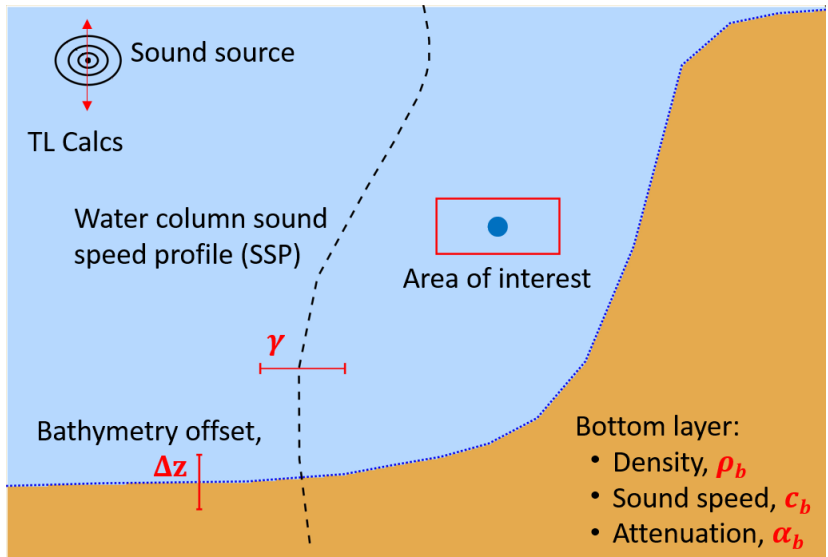
Problem: Efficient estimation of the probability density function (PDF) of transmission loss (TL) in uncertain ocean environments

Transmission Loss, $TL = 20 \log_{10} \left(\frac{P_{source}}{P_{receiver}} \right)$, is useful for naval applications.

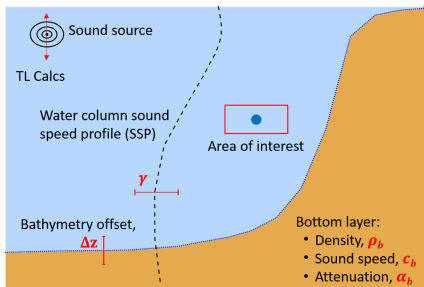


TL uncertainty is important for those making decisions based on TL, but traditional methods are slow and expensive.

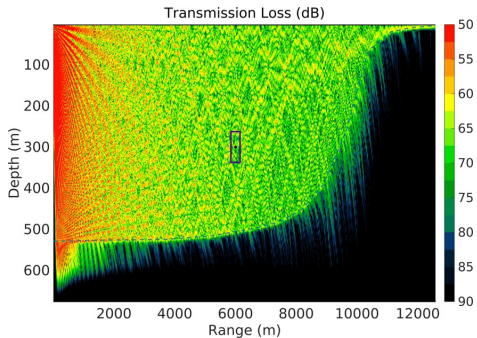
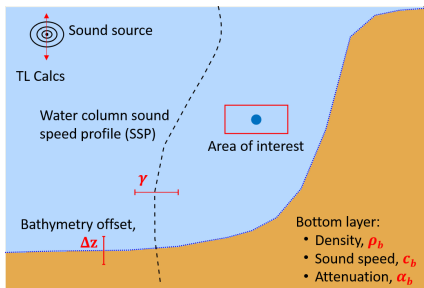
Consider an uncertain ocean environment



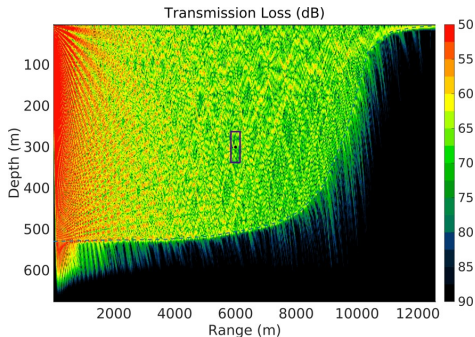
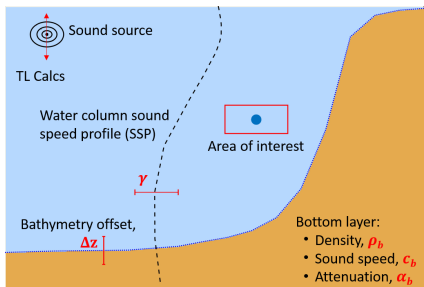
Consider an uncertain ocean environment and corresponding TL field



Consider an uncertain ocean environment and corresponding TL field



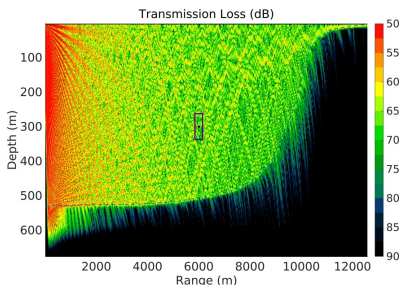
Consider an uncertain ocean environment and corresponding TL field



The idea is that variations in the TL field due to environmental fluctuations are represented by surrounding spatial variations in TL.

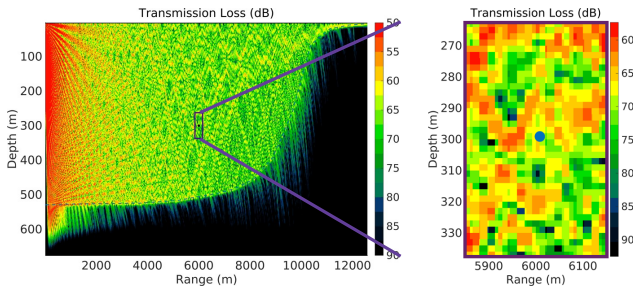
We estimate a Probability Density Function (PDF) of TL at points of interest, using TL from the surrounding areas

The *Area Statistics* technique:



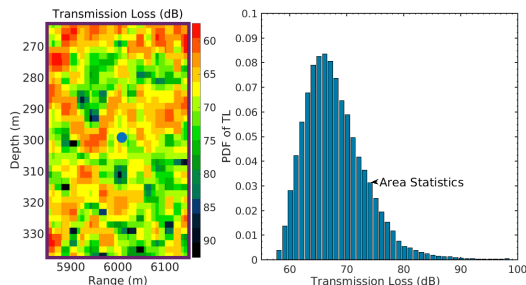
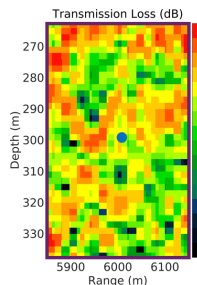
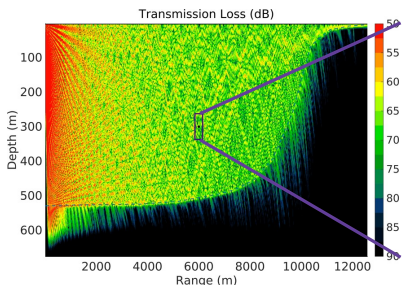
We estimate a Probability Density Function (PDF) of TL at points of interest, using TL from the surrounding areas

The *Area Statistics* technique:



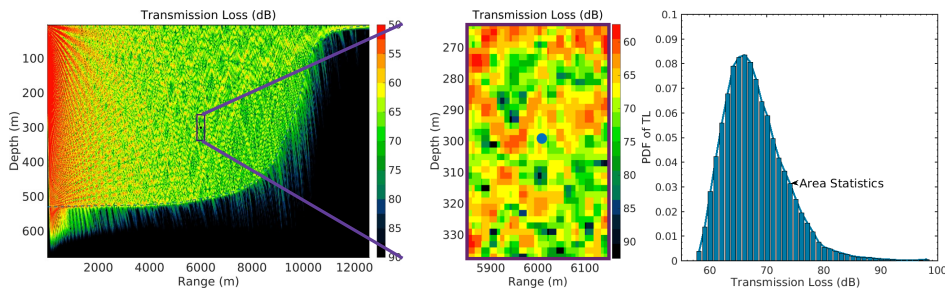
We estimate a Probability Density Function (PDF) of TL at points of interest, using TL from the surrounding areas

The *Area Statistics* technique:



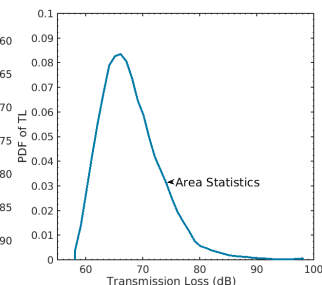
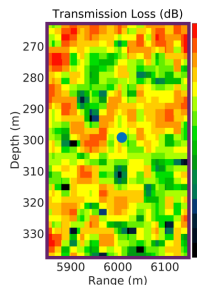
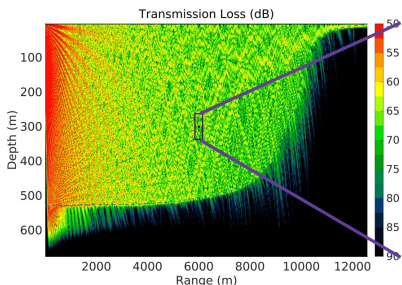
We estimate a Probability Density Function (PDF) of TL at points of interest, using TL from the surrounding areas

The *Area Statistics* technique:



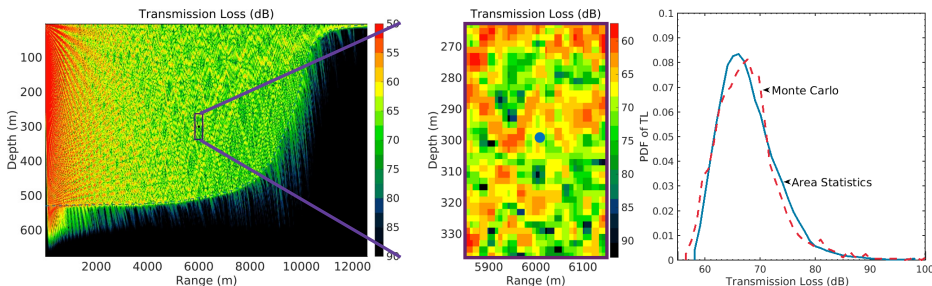
We estimate a Probability Density Function (PDF) of TL at points of interest, using TL from the surrounding areas

The *Area Statistics* technique:



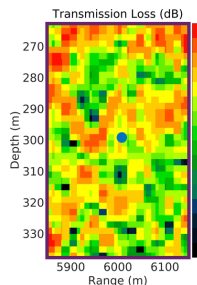
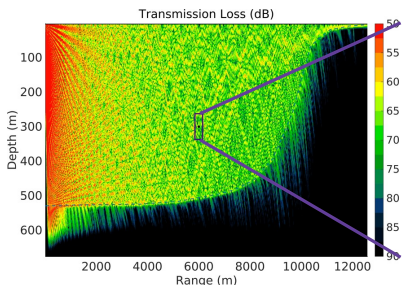
Area statistics TL PDFs are compared to Monte Carlo TL PDFs via L_1 error norm

The *Area Statistics* technique:

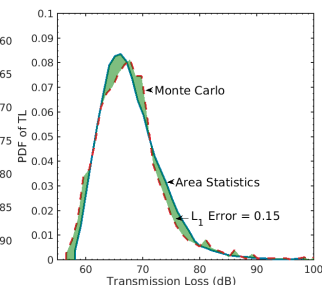


Area statistics TL PDFs are compared to Monte Carlo TL PDFs via L_1 error norm

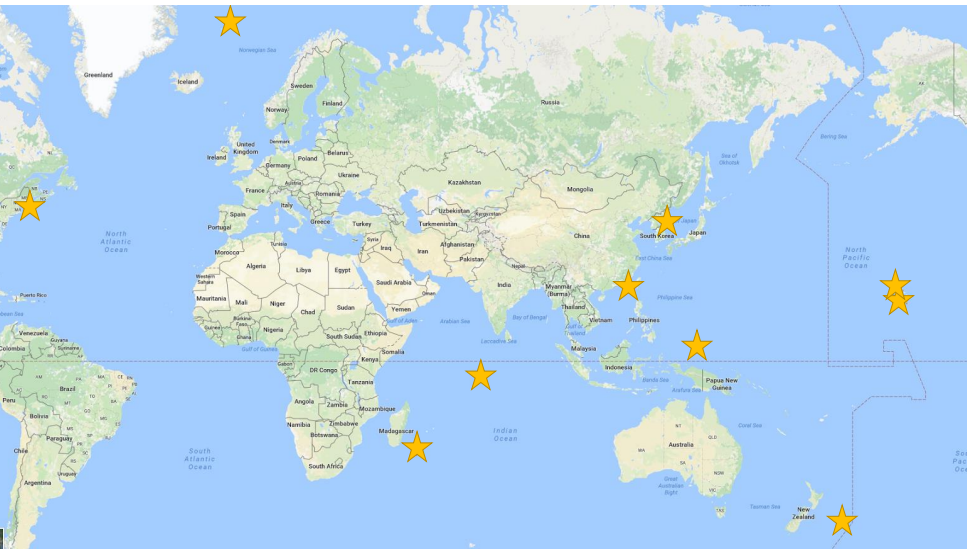
The *Area Statistics* technique:



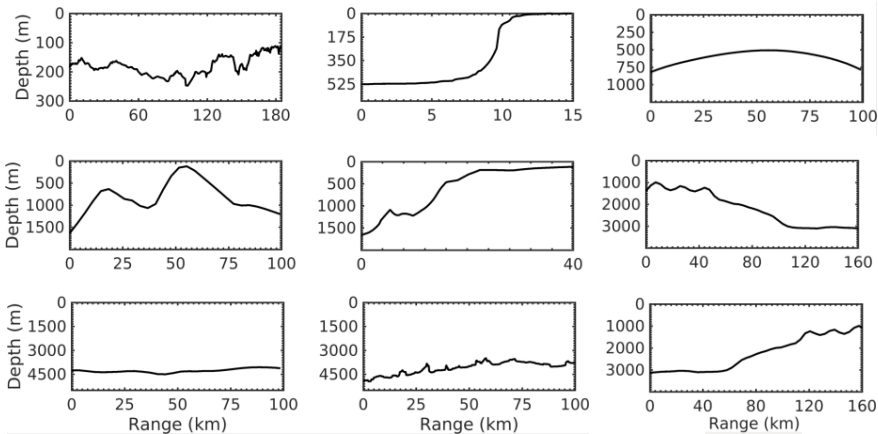
$$L_1 = \int_{-\infty}^{+\infty} |\text{PDF}_{MC}(TL) - \text{PDF}_{AS}(TL)| d(TL)$$



Area statistics TL PDFs are compared to 2000 sample Monte Carlo-generated PDFs with randomized environmental parameters



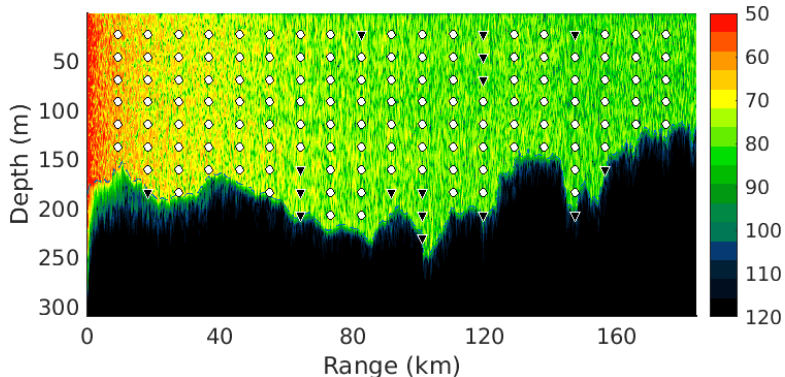
Area statistics TL PDFs are compared to 2000 sample Monte Carlo-generated PDFs with randomized environmental parameters



Results: Area statistics performance in multiple environments

Source: $f_s = 200$ Hz, $z_s = 137$ m (450 ft)

- ▼ $L_1 \geq 0.5$ (fail)
- $L_1 < 0.5$ (Pass)

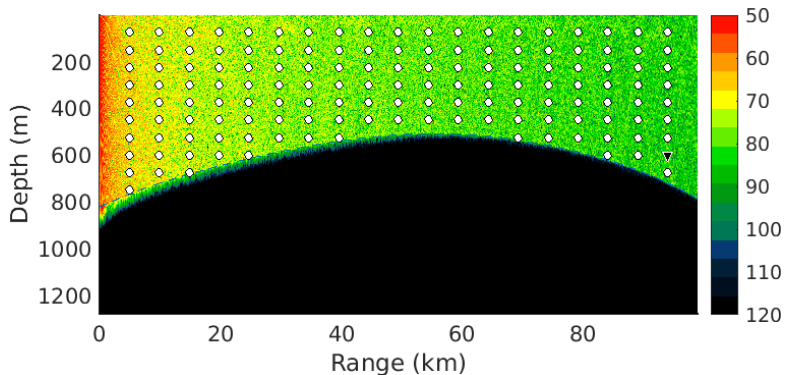


Engineering-level accuracy (L_1 error < 0.5) is achieved in most locations

Results: Area statistics performance in multiple environments

Source: $f_s = 200$ Hz, $z_s = 137$ m (450 ft)

- ▼ $L_1 \geq 0.5$ (fail)
- $L_1 < 0.5$ (Pass)

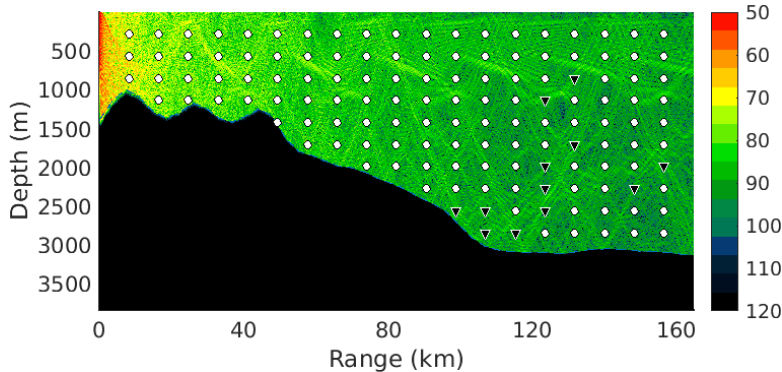


Engineering-level accuracy (L_1 error < 0.5) is achieved in most locations

Results: Area statistics performance in multiple environments

Source: $f_s = 200$ Hz, $z_s = 137$ m (450 ft)

- ▼ $L_1 \geq 0.5$ (fail)
- $L_1 < 0.5$ (Pass)

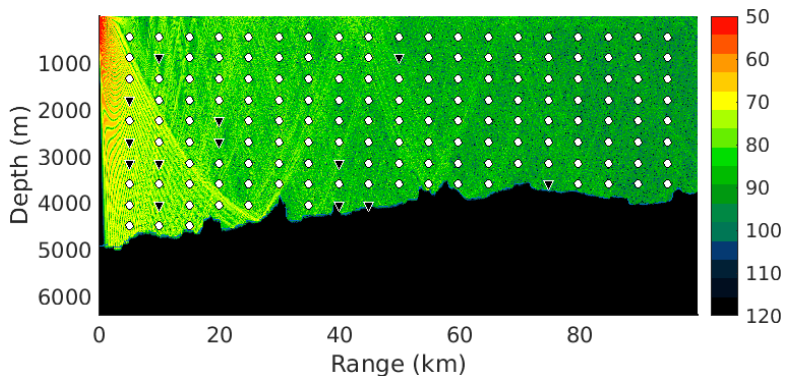


Engineering-level accuracy (L_1 error < 0.5) is achieved in most locations

Results: Area statistics performance in multiple environments

Source: $f_s = 200$ Hz, $z_s = 137$ m (450 ft)

- ▼ $L_1 \geq 0.5$ (fail)
- $L_1 < 0.5$ (Pass)

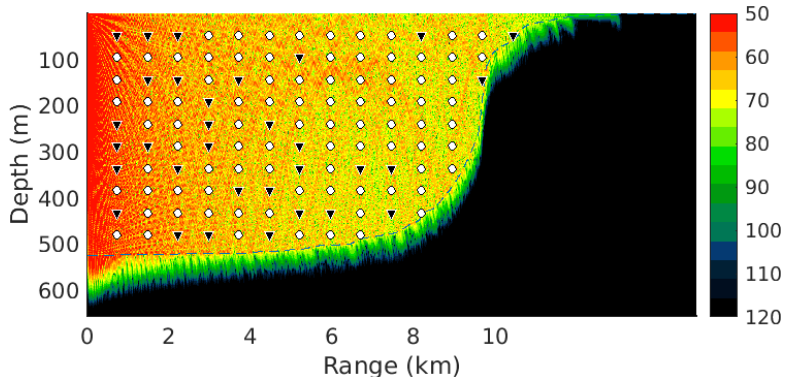


Engineering-level accuracy (L_1 error < 0.5) is achieved in most locations

Results: Area statistics performance in multiple environments

Source: $f_s = 200$ Hz, $z_s = 137$ m (450 ft)

- ▼ $L_1 \geq 0.5$ (fail)
- $L_1 < 0.5$ (Pass)



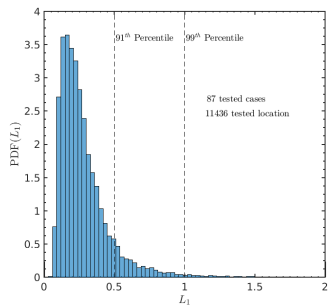
Engineering-level accuracy (L_1 error < 0.5) is achieved in most locations
in most environments

Area statistics is fast and usually engineering-level accurate

Overall Performance:

87 environment-source cases & 11000+ test locations

- Engineering-level accurate (L_1 error < 0.5) in 91% of test locations
- 0.28 average L_1 error
- 1.6 million times less computational effort than Monte Carlo PDFs, on average
- Appropriate for real-time applications:
TL PDFs generated in milliseconds on a PC



Limitations

- Performs poorly near the sound source in environments with little sound speed uncertainty

PhD Contributions

PhD Contributions

Part I:

- 1.) I developed a novel model of an ultrasound driven alveolus.

PhD Contributions

Part I:

- 1.) I developed a novel model of an ultrasound driven alveolus.
- 2.) I proposed Vorticity-driven alveolar strain as a mechanism for DUS-induced lung hemorrhage and demonstrated that potentially damaging strains are plausible for diagnostically relevant ultrasound conditions, based on simulations.

PhD Contributions

Part I:

- 1.) I developed a novel model of an ultrasound driven alveolus.
- 2.) I proposed Vorticity-driven alveolar strain as a mechanism for DUS-induced lung hemorrhage and demonstrated that potentially damaging strains are plausible for diagnostically relevant ultrasound conditions, based on simulations.
- 3.) I theoretically demonstrated fluid-fluid interface perturbation growth due to acoustically-generated baroclinic vorticity, and showed that the growth scales with circulation density and exhibit power-law growth in time.

PhD Contributions

Part I:

- 1.) I developed a novel model of an ultrasound driven alveolus.
- 2.) I proposed Vorticity-driven alveolar strain as a mechanism for DUS-induced lung hemorrhage and demonstrated that potentially damaging strains are plausible for diagnostically relevant ultrasound conditions, based on simulations.
- 3.) I theoretically demonstrated fluid-fluid interface perturbation growth due to acoustically-generated baroclinic vorticity, and showed that the growth scales with circulation density and exhibit power-law growth in time.
- 4.) I showed that long-term fluid interface perturbation growth depends on the driving waveform, due to the transient morphology of the interface. This suggests that long-term interface growth may be controllable.

PhD Contributions

Part I:

- 1.) I developed a novel model of an ultrasound driven alveolus.
- 2.) I proposed Vorticity-driven alveolar strain as a mechanism for DUS-induced lung hemorrhage and demonstrated that potentially damaging strains are plausible for diagnostically relevant ultrasound conditions, based on simulations.
- 3.) I theoretically demonstrated fluid-fluid interface perturbation growth due to acoustically-generated baroclinic vorticity, and showed that the growth scales with circulation density and exhibit power-law growth in time.
- 4.) I showed that long-term fluid interface perturbation growth depends on the driving waveform, due to the transient morphology of the interface. This suggests that long-term interface growth may be controllable.
- 5.) I related experimentally-determined ultrasound bioeffects thresholds to calculated cavitation metrics.

PhD Contributions

Part I:

- 1.) I developed a novel model of an ultrasound driven alveolus.
- 2.) I proposed Vorticity-driven alveolar strain as a mechanism for DUS-induced lung hemorrhage and demonstrated that potentially damaging strains are plausible for diagnostically relevant ultrasound conditions, based on simulations.
- 3.) I theoretically demonstrated fluid-fluid interface perturbation growth due to acoustically-generated baroclinic vorticity, and showed that the growth scales with circulation density and exhibit power-law growth in time.
- 4.) I showed that long-term fluid interface perturbation growth depends on the driving waveform, due to the transient morphology of the interface. This suggests that long-term interface growth may be controllable.
- 5.) I related experimentally-determined ultrasound bioeffects thresholds to calculated cavitation metrics.

Part II:

- 6.) I developed a technique to estimate TL PDF's in *most* uncertain environments that is real-time appropriate.

Possible future directions

Possible future directions

Part I: Enhance direct relevance to DUS

- Add relevant physical effects physics (e.g., viscosity) and adapt code to be less computationally intensive

Possible future directions

Part I: Enhance direct relevance to DUS

- Add relevant physical effects physics (e.g., viscosity) and adapt code to be less computationally intensive
- Use experimental data as input waves and geometry

Possible future directions

Part I: Enhance direct relevance to DUS

- Add relevant physical effects physics (e.g., viscosity) and adapt code to be less computationally intensive
- Use experimental data as input waves and geometry
- Perform simulations using previously performed experiments to look for trends relating the observed dynamics to experimentally observed bioeffects

Possible future directions

Part I: Enhance direct relevance to DUS

- Add relevant physical effects physics (e.g., viscosity) and adapt code to be less computationally intensive
- Use experimental data as input waves and geometry
- Perform simulations using previously performed experiments to look for trends relating the observed dynamics to experimentally observed bioeffects

Part II: Overcome Area Statistics' limitations in low SSP variability environments

- Use neural networks to predict cases where area statistics is likely to fail based on known uncertainties and environmental properties and adapt PDFs appropriately.

THANKS!

- Beyer, Robert T. 1974. *Nonlinear Acoustics*.
- Brouillette, Martin. 2002. The Richtmyer-Meshkov Instability. *Annu. rev. fluid mech.*, **34**(1), 445–468.
- Child, S.Z., Hartman, C.L., Schery, L.A., & Carstensen, E.L. 1990. Lung damage from exposure to pulsed ultrasound. *Ultrasound med. biol.*, **16**(8), 817–825.
- Drake, Paul. 2006. *High-Energy-Density Physics*. Shock Wave and High Pressure Phenomena. Springer Berlin Heidelberg.
- Heifetz, E., & Mak, J. 2015. Stratified shear flow instabilities in the non-Boussinesq regime. *Phys. fluids*, **27**(8), 086601.
- Henry de Frahan, Marc T., Varadan, Sreenivas, & Johnsen, Eric. 2015. A new limiting procedure for discontinuous Galerkin methods applied to compressible multiphase flows with shocks and interfaces. *J. comput. phys.*, **280**(jan), 489–509.
- Lichtenstein, Daniel A. 2009. Ultrasound examination of the lungs in the intensive care unit. *Pediatr. crit. care med.*, **10**(6), 693–698.
- Miller, DL. 2012. Induction of Pulmonary Hemorrhage in Rats During Diagnostic Ultrasound. *Ultrasound med. biol.*, **38**(8), 1476–1482.
- O'Brien, William D. W.D., & Zachary, J.F. 1997. Lung damage assessment from exposure to pulsed-wave ultrasound in the rabbit, mouse, and pig. *Ieee trans. ultrason. ferroelectr. freq. control*, **44**(2), 473–485.
- Ochs, Matthias, Nyengaard, Jens R., Jung, Anja, Knudsen, Lars, Voigt, Marion, Wahlers, Thorsten, Richter, Joachim, & Gundersen, Hans Jørgen G. 2004. The Number of Alveoli in the Human Lung. *Am. j. respir. crit. care med.*, **169**(1), 120–124.

Tarantal, Alice F., & Canfield, Don R. 1994. Ultrasound-induced lung hemorrhage in the monkey. *Ultrasound med. biol.*, **20**(1), 65–72.

Wei, Kevin, Le, Elizabeth, Bin, Jian-Ping, Coggins, Matthew, Thorpe, Jerrel, & Kaul, Sanjiv. 2001. Quantification of renal blood flow with contrast-enhanced ultrasound. *J. am. coll. cardiol.*, **37**(4), 1135–1140.

West, J B, Tsukimoto, K, Mathieu-Costello, O, & Prediletto, R. 1991. Stress failure in pulmonary capillaries. *J. appl. physiol.*, **70**(4), 1731–1742.

BACKUP SLIDES

Governing Equations

Euler equations of fluid motion

$$\frac{\partial \rho}{\partial t} + \frac{\partial(\rho u)}{\partial x} + \frac{\partial(\rho v)}{\partial y} = 0, \quad \text{Continuity}$$

$$\frac{\partial \rho u}{\partial t} + \frac{\partial}{\partial x} (\rho u^2 + p) + \frac{\partial}{\partial y} (\rho u v) = 0, \quad x\text{-momentum}$$

$$\frac{\partial \rho v}{\partial t} + \frac{\partial}{\partial x} (\rho u v) + \frac{\partial}{\partial y} (\rho v^2 + p) = 0, \quad y\text{-momentum}$$

$$\frac{\partial E}{\partial t} + \frac{\partial}{\partial x} [u(E + p)] + \frac{\partial}{\partial y} [v(E + p)] = 0, \quad \text{Energy}$$

Stiffened equation of state

$$E = \frac{\rho(u^2 + v^2)}{2} + \frac{p + \gamma B}{\gamma - 1}.$$

Advection equations for γ , B prevent interface pressure oscillations.

$$\frac{\partial}{\partial t} \left(\frac{\gamma B}{\gamma - 1} \right) + u \frac{\partial}{\partial x} \left(\frac{\gamma B}{\gamma - 1} \right) + v \frac{\partial}{\partial y} \left(\frac{\gamma B}{\gamma - 1} \right) = 0,$$

$$\frac{\partial}{\partial t} \left(\frac{1}{\gamma - 1} \right) + u \frac{\partial}{\partial x} \left(\frac{1}{\gamma - 1} \right) + v \frac{\partial}{\partial y} \left(\frac{1}{\gamma - 1} \right) = 0$$

Interface treatment

Interface thickness parameter:

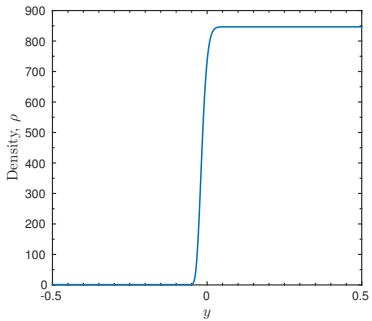
$$\delta = 0.08\lambda$$

Normalized distance from interface:

$$d = \frac{\delta + y(x)_{interface} - y}{2\delta}$$

Volume fraction:

$$y_0 = \begin{cases} 1 \\ \exp \left(\log (10^{-16}) |d|^8 \right) \\ 0 \end{cases}$$

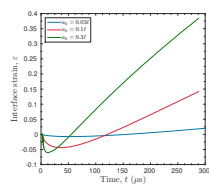
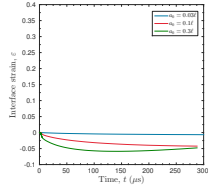
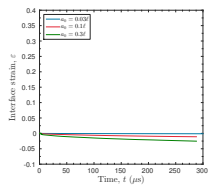
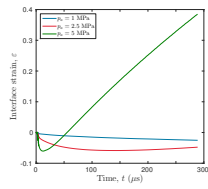
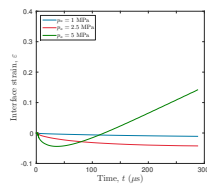
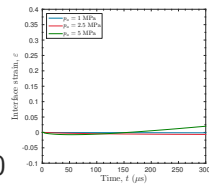
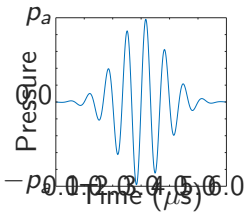
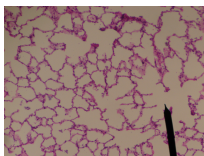
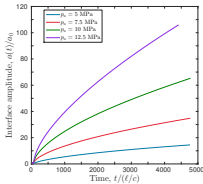
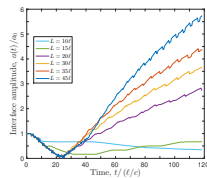
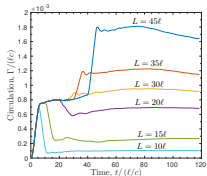


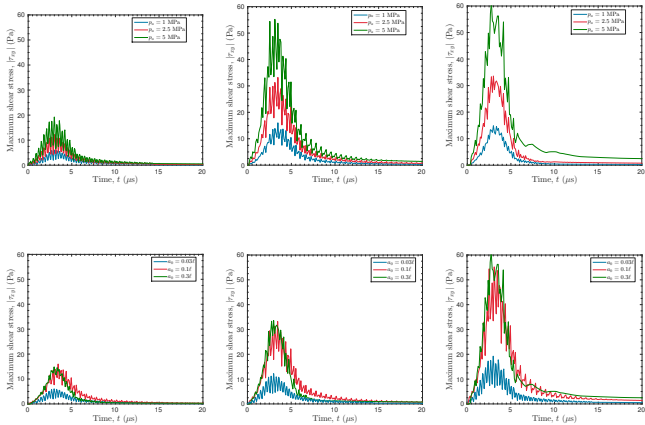
Radiation Pressure

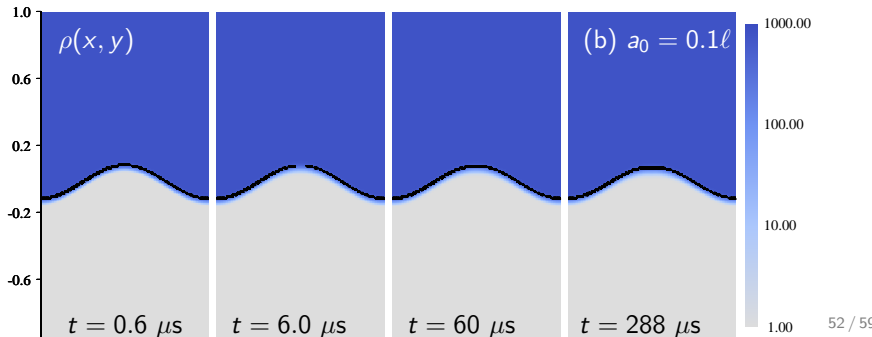
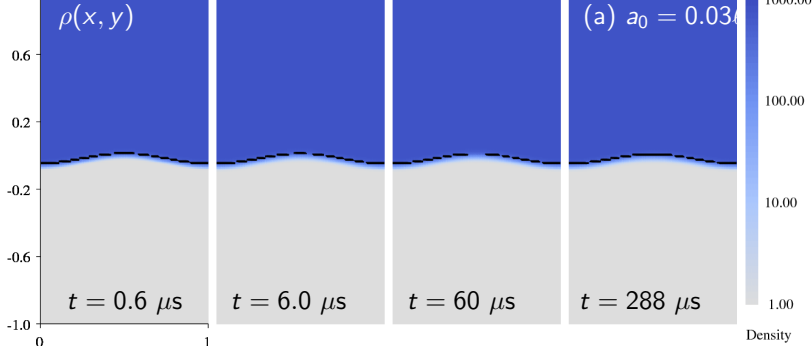
$$P_{net} = \frac{\Delta p_a}{2} \left[1 - \frac{c_w}{c_a} + \frac{(\rho c)_a - (\rho c)_w}{(\rho c)_a (\rho c)_w} \right] \text{ Beyer (1974)}$$

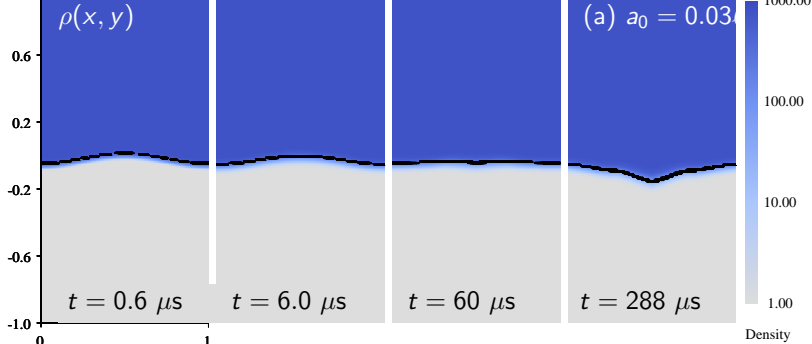
Stress failure in the lungs:

Rabbit lungs under transmural pressure: $\approx 5.2 \text{ kPa}$ (West *et al.*, 1991);

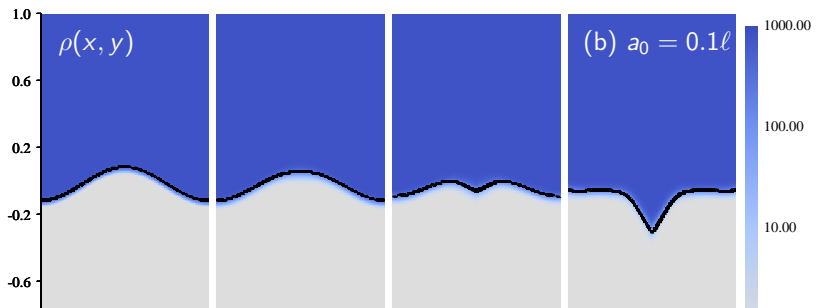


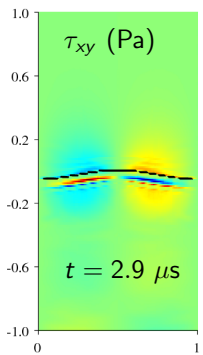




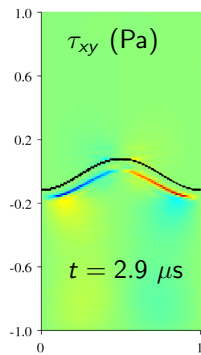


(a) $a_0 = 0.03\ell$

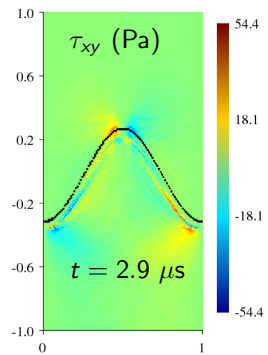




$$a_0 = 0.03\ell$$



$$a_0 = 0.1\ell$$



$$a_0 = 0.3\ell$$

Figure : Evolution of the viscous stress field for the $p_a = 5$ MPa wave. Contour plots of the Newtonian viscous stress τ_{xy} in Pascals are shown for each initial perturbation amplitude, at $t = 5$, near the point when the maximum stress occurs. In Figures a, b, and c $a_0 = 0.03\ell$, 0.1ℓ , and 0.3ℓ respectively.

Argument against viscosity - viscous length scales

$$\nu_w = 0.7 \mu\text{m}^2/\text{s}, \quad \nu_a = 16.6 \mu\text{m}^2/\text{s}, \quad f_c = \mathcal{O}(10^6) \text{ Hz}$$

$$\sqrt{\nu_{air}/f_c} = 4\mu \text{ m} = \mathcal{O}(10^{-6}) \ll L_{alveolus} = \mathcal{O}(10^{-4})$$

$$\sqrt{\nu_{air,ND} t} \approx 0.5 < a(t) - a_0 \approx 4 \text{ at } t = 1000$$

Therefore the scale of the viscous effect is smaller than the scale of the problem we are looking at, but may be important at late times.

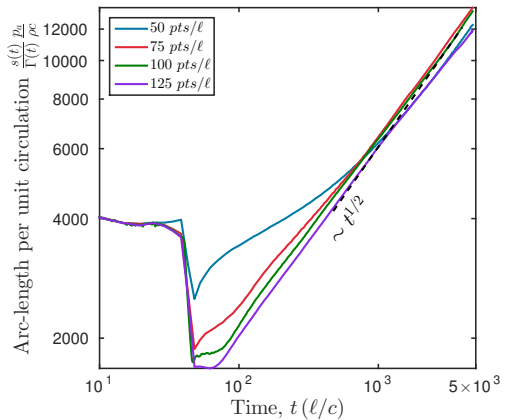
Dimensional Numbers

- Let $\lambda_{alveolus} = 100\mu \text{ m}$, $u_0 = c_{air} = 343 \text{ m}$, $v_0 = \langle a(t) \rangle \approx 0.65 \text{ m/s}$,
 $u_{intf}(t=20) = 12.8 \text{ m/s}$, $G = 1 \text{ kPa}$
- $\lambda_{alveolus} = 100\mu \text{ m}$, $u_0 = c_{air} = 343 \text{ m}$, $v_0 = \langle a(t) \rangle \approx 0.65 \text{ m/s}$
- $t = 1 \rightarrow t_{dim} = 0.292\mu \text{ s}$

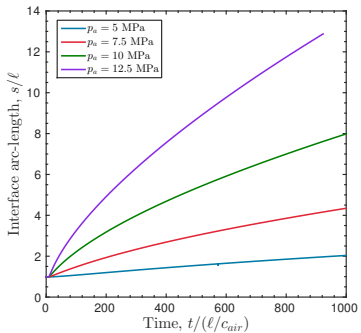
Dimensionless Numbers

- $Fr = \frac{u_0}{\sqrt{g_0 \lambda}} \approx 11000$
- $Fr = \frac{v_0}{\sqrt{g_0 \lambda}} \approx 21$
- $Ca = \frac{\rho u_{intf}^2}{G_{Alv}} = 163$

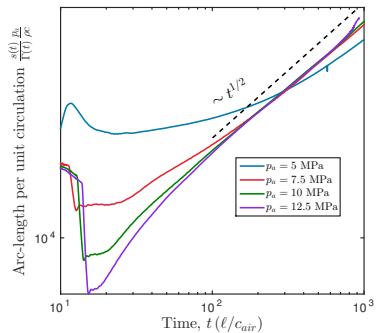
Convergence test



The interface arc length per unit circulation $s(t)/\Gamma(t)$ grows approximately as $t^{1/2}$ and scales with wave amplitude p_a .

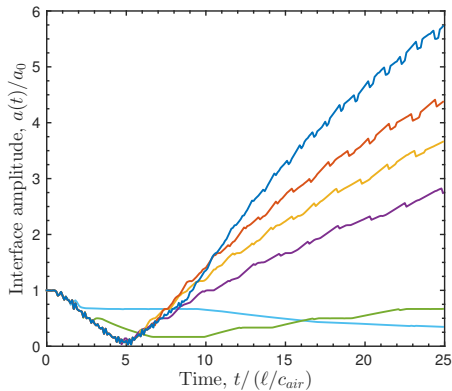


(a) Constant scaling: $s(t)/\ell$

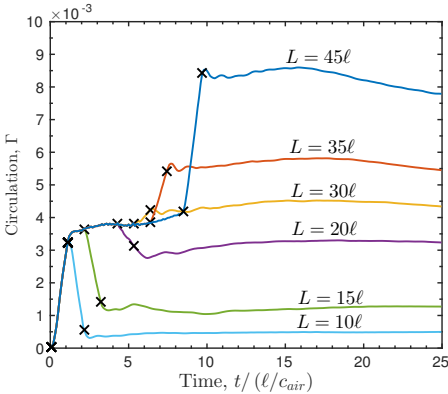


(b) Vortex strength scaling: $\frac{s(t)}{\Gamma(t)} \frac{p_a}{\rho c}$

The circulation deposited and therefore late time perturbation growth depend heavily on time-dependent wave features



(a) $a(t)/a_0$



(b) $\Gamma(t)$

The interface amplitude (left) and circulation (right) histories for waves of varying total length L and elevated static pressure duration between the expansion and compression. Here we show results for $L = 45\ell$ (blue), $L = 35\ell$ (orange), $L = 30\ell$ (yellow), $L = 20\ell$ (purple), $L = 15\ell$ (green), $L = 10\ell$ (light blue)

Summary and conclusions

Summary:

- We studied the interaction of finite-duration acoustic waves with gas-liquid interfaces.

Conclusions

- Baroclinic vorticity is generated acoustic wave-interface interactions
- This vorticity appears to deforming perturbed liquid-gas interfaces.
- The interface perturbation grows as $t^{3/5}$ and scales with linear circulation density along the interface Γ_0/s_0 .
- The interface arc length per unit circulation $s(t)/\Gamma(t)$ grows approximately as $t^{1/2}$ and scales with wave amplitude p_a .
- This may be a mechanism for ultrasound-induced alveolar strain and hemorrhage and should be studied further.